

Limits and Prospects of Nb₃Sn Accelerator Magnets

Supervisors:

Emanuela Barzi

Alexander Zlobin

Student:

Marco Danuso

Outline

I. A Parametric Model for Electromechanical Effects in HFMs

- Linear
- Analytic solutions
- Limits of HFMs

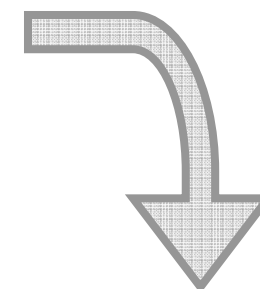


Results suggest the need of

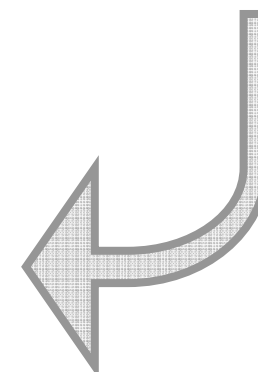
II. An experiment for equivalent stress in HFMs

III. A FEM Elastoplastic Model

- Accuracy of parametric model
- Non-linear phenomena



The P.M. was checked and integrated with



Outline

I. A Parametric Model for Electromechanical Effects in HFMs

- Linear
- Analytic solutions
- Limits of HFMs

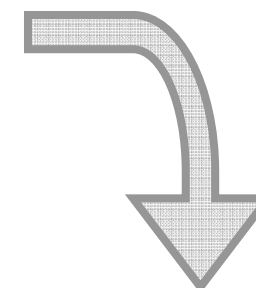


Results suggest the need of

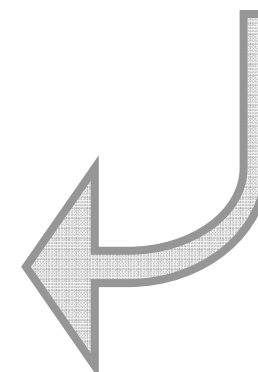
II. An experiment for equivalent stress in HFMs

III. A FEM Elastoplastic Model

- Accuracy of parametric model
- Non-linear phenomena



The P.M. was checked and integrated with



I. A Parametric Model for Electromechanical Effects in HFMs – Outline

- Introduction
 - Magnet Requirements
 - Goals of analysis
 - Overview of existing models (Caspi05 and Fessia06)
- Model description
 - Model geometry
 - Material properties
 - Magnetic Field
 - Mechanical Model
 - Field Quality
- Results
 - Magnet performance
 - Multiaxiality of the stress tensor
 - Field quality

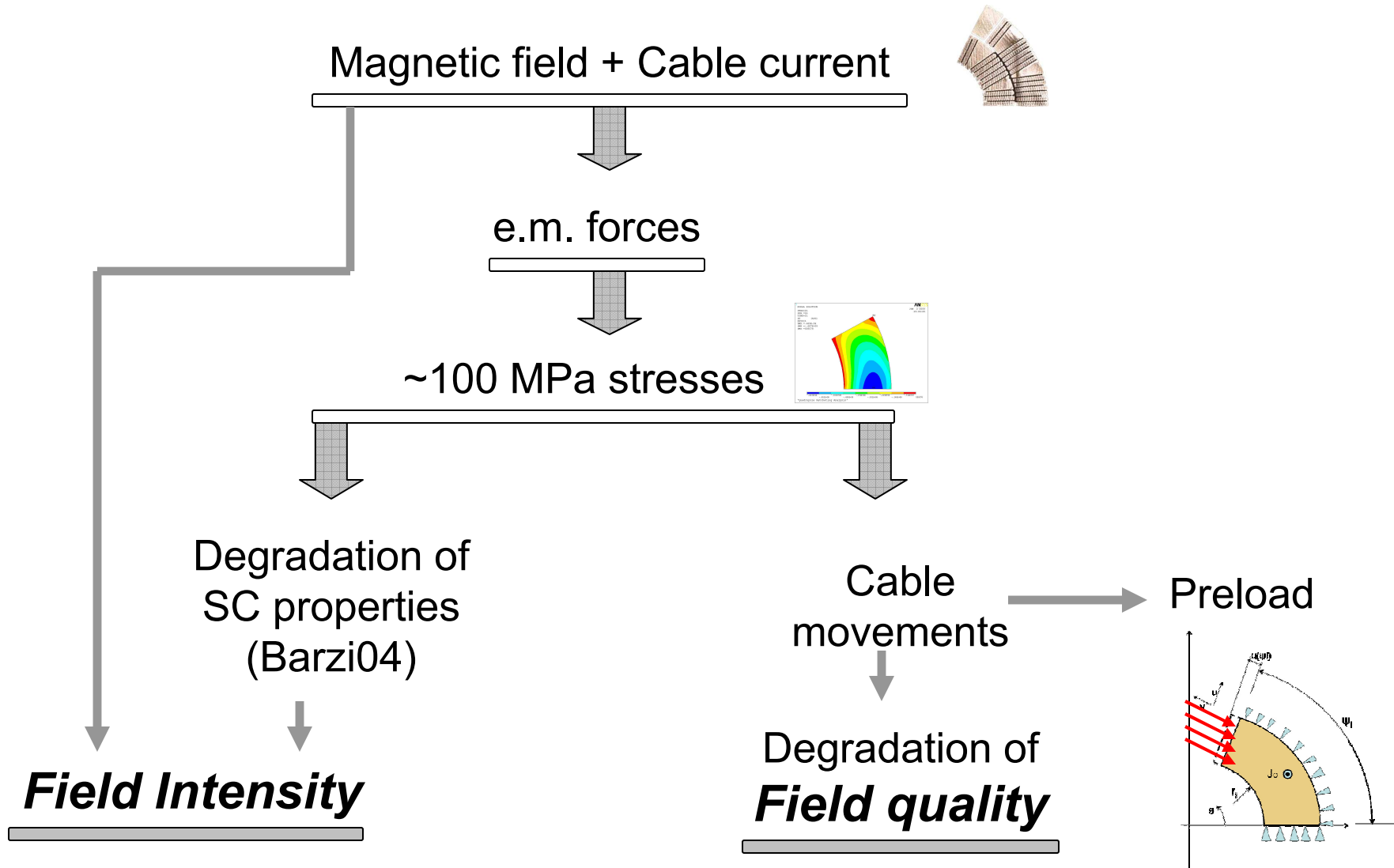
Magnet requirements

Field Intensity: { *Dipoles:* the attainable beam energy is proportional to the bending magnetic field
Quadrupoles: the focusing elements must be kept as short as possible

Field Quality: a high *field quality* is needed to store an intense particle beam for many hours

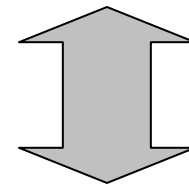
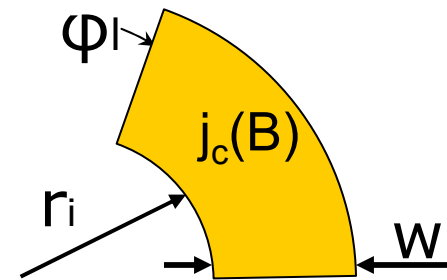
($\Delta b_i < 10^{-4}$ for a storage time of 10 – 20 hours)

Magnet requirements



Goals of analysis

- analyse how *stresses, field intensity and quality* depend on the *coil geometry* and on the *superconducting material*
- address how far the engineering of HFMs can be pushed
- identify issues and limitations of their employment

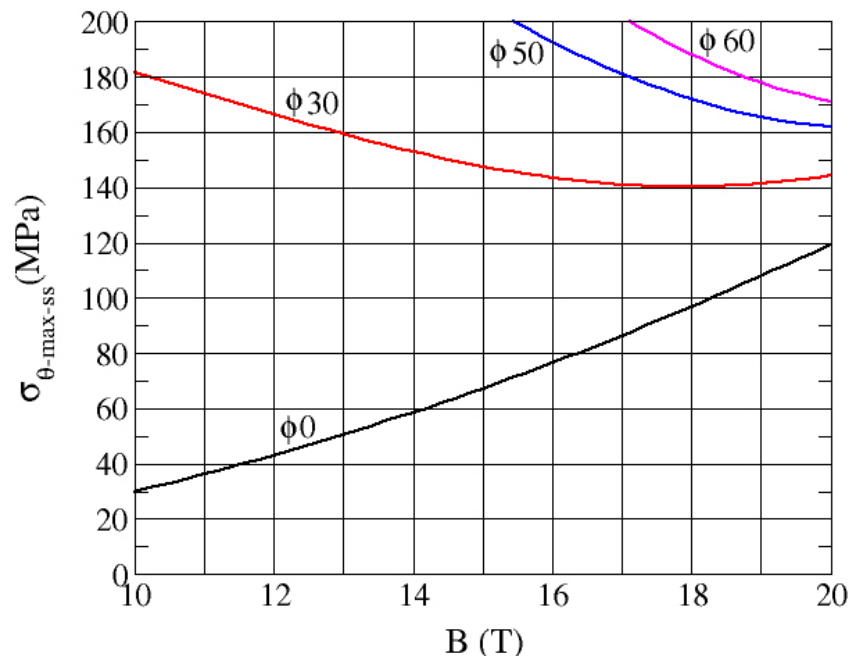


$B_c, G_c, \sigma_{max}, b_i$

Overview of existing models

Caspi05 Dipoles

- The bore is round and the coil is a thick cylinder
- The current density is $J \cdot \cos\theta$ (*pure dipole*)
- There is no ferromagnetic material nearby

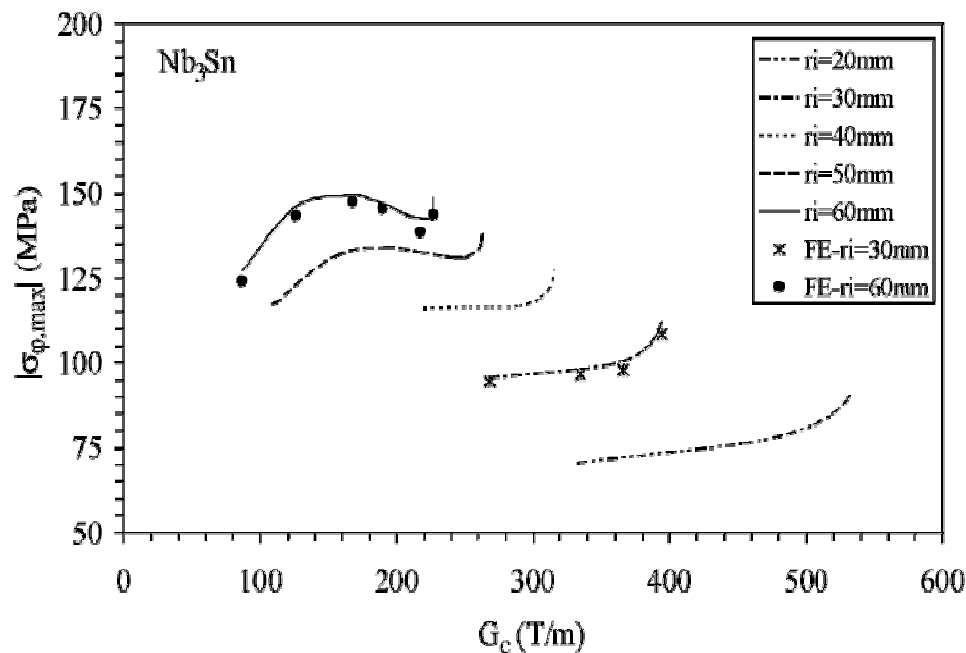
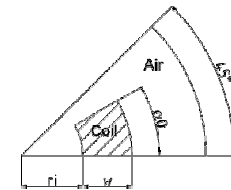


- B_c independent of bore diameter
- Coil area increases tenfold from $14 T$ to $18 T$
- The level of stress represents a practical limit for practical Nb_3Sn coils

Overview of existing models

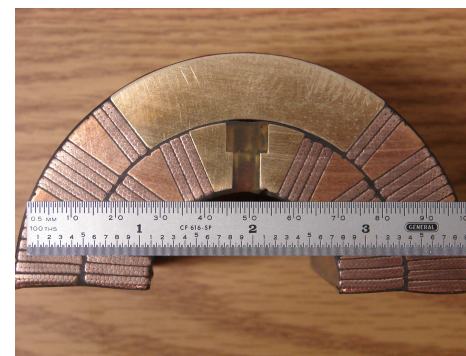
Fessia06 Quadrupoles

- Coil layout made up of a sector of ang. extension $\alpha_0=30^\circ$
- Uniform current density
- There is no ferromagnetic material nearby

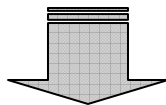


- The stress increases for larger apertures
- Maximum stress is just below 150 MPa for $r_i=60$ mm
- σ_θ does not increase monotonically with G_c : it displays a local maximum

Model Geometry



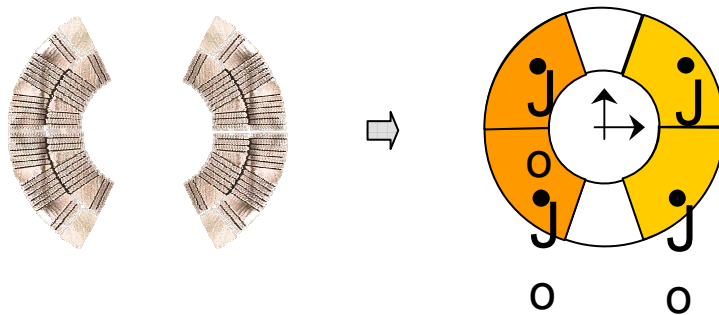
- Magnets are much longer along the axis ($\sim 8m$) than wide ($< 0.1m$)
- The conductors run parallel to the axis
- Recent coil designs move the highest field point to the straight section
- The deviation of the beam from a straight line is negligible



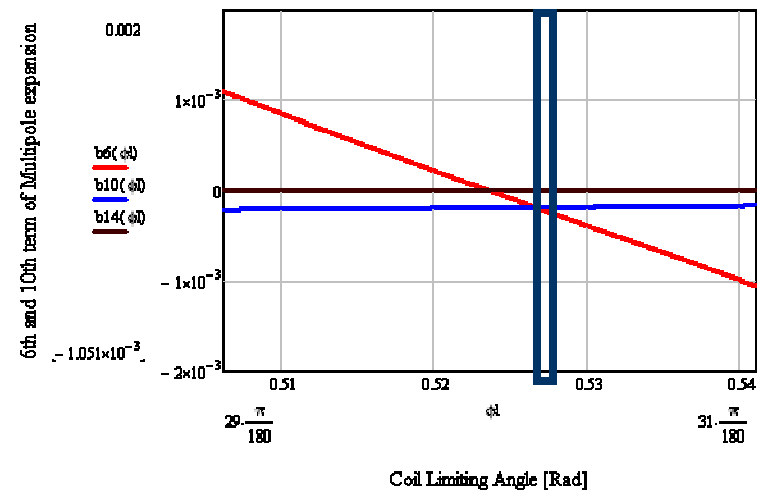
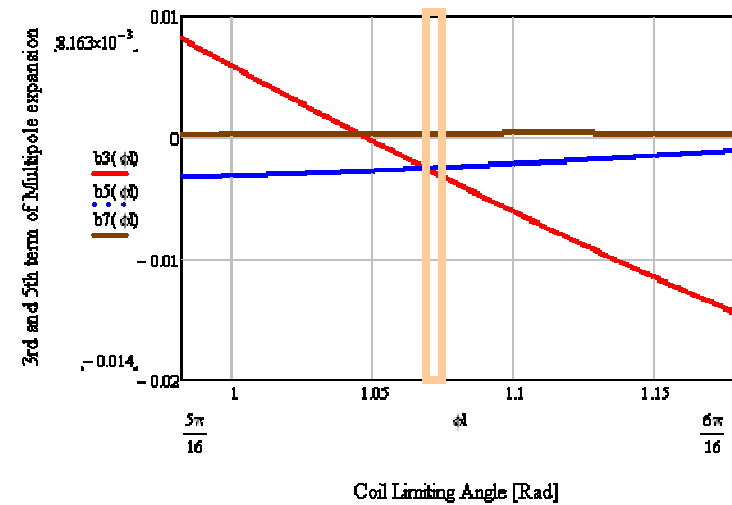
2D Magnetic field

Theory of analytic functions

Model geometry – coil sector



- sector of uniform current density, more realistic than a $\cos\theta$ distribution (*Caspi05*), but more elaborate model
- Angular extension of 60° for dipoles and 30° for quadrupoles, thus canceling the first allowed field harmonic



Material Properties: Critical Surface

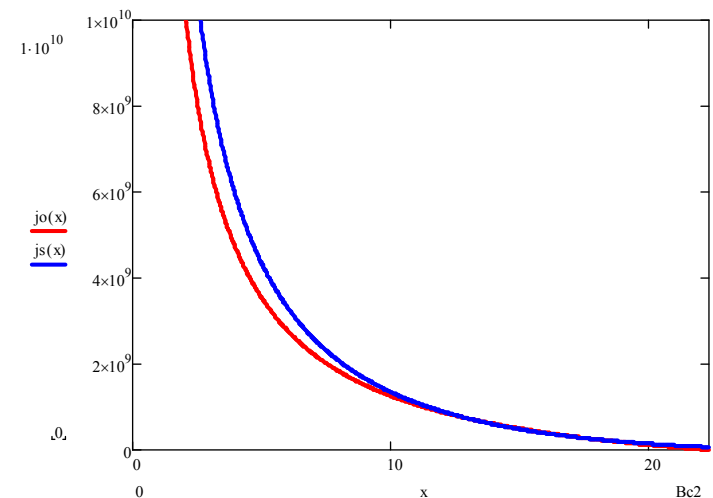
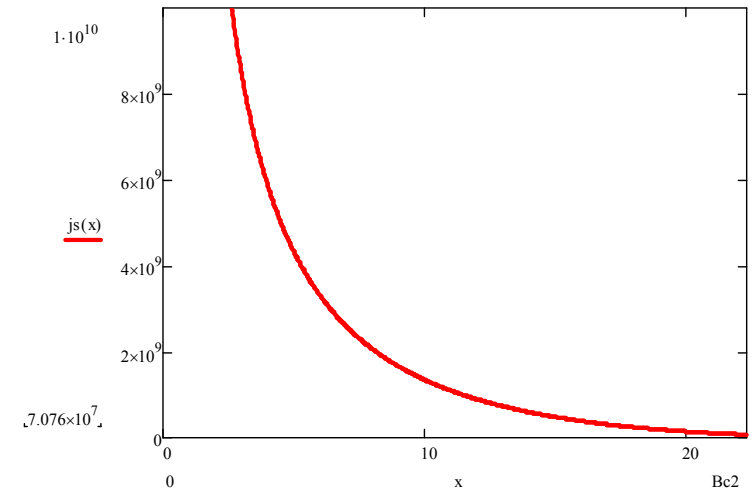
- Dipoles: Summers' fit of the critical surface

$$J_s c(B, T) = C B^{-1/2} (1 - t^2)^2 b^{-1/2} (1 - b)^2$$

$$t = \frac{T}{T_{c0}} \quad b = \frac{B}{B_{c2}(T)}$$

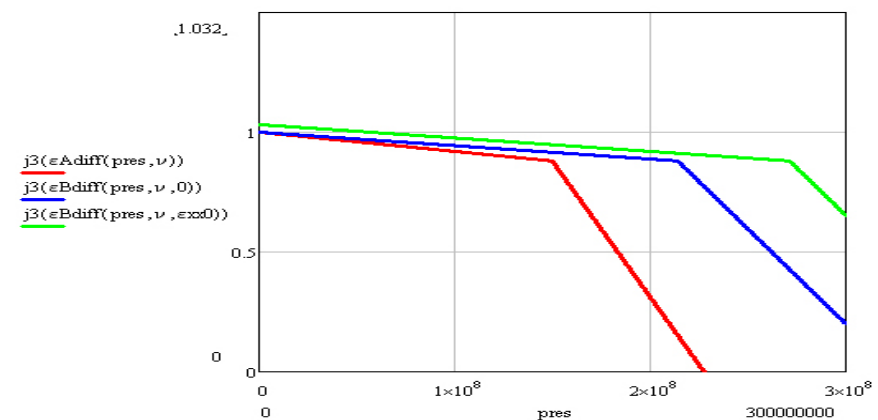
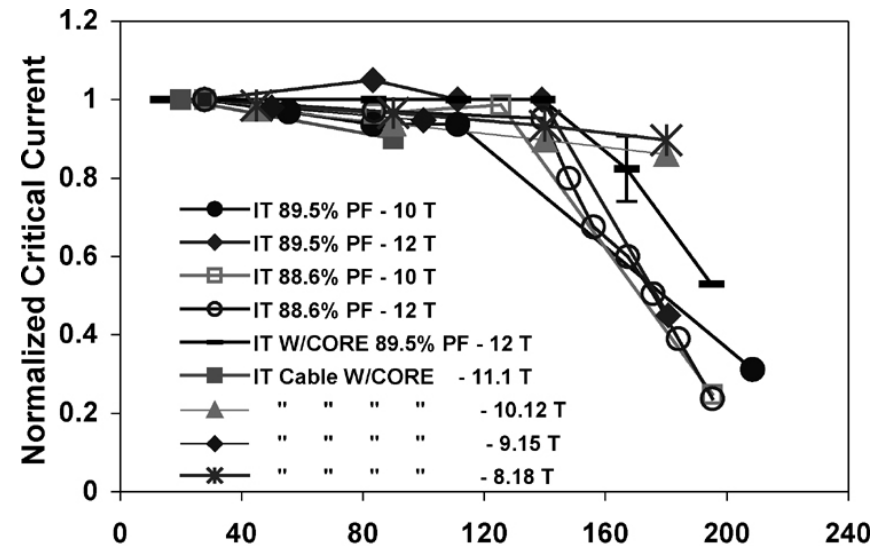
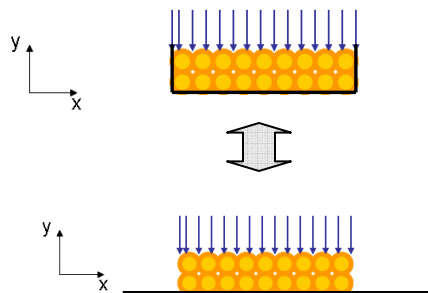
- Quadrupoles: hyperbolic fit proposed by Todesco06 ($e < 5\%$ for $11 T < B < 17 T$)

$$J_s c(B) = c \left(\frac{b}{B} - 1 \right) \quad B < b$$



Material Properties: Strain sensitivity

- Superconductor's properties are sensitive to transverse pressure (Barzi04)
- In the presence of multiaxiality, an equivalent strain is needed
- A simple experiment was proposed, observations will follow

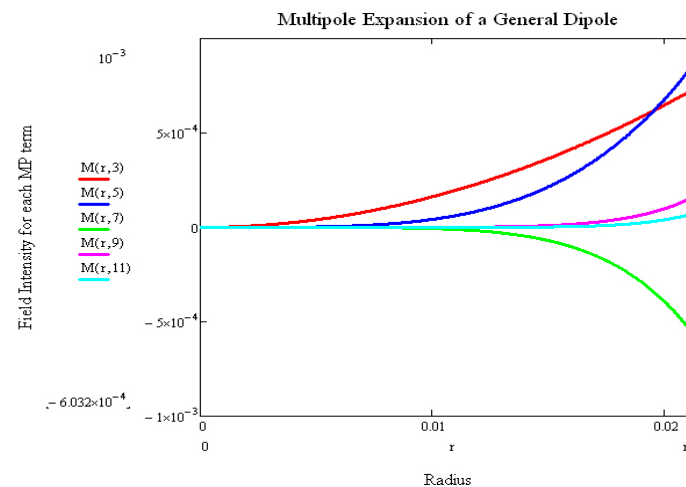


Magnetic field

- The vector potential **A** can be expressed analytically both for dipoles and quadrupoles
- Analytical expression of **B** derived from the vector potential **A**
- Terms with $n \geq 3$ for dipoles and $n \geq 6$ for quadrupoles were neglected
- The amplitude of the terms goes to 0 as $1/n^3$
- The maximum field is evaluated with a $\sim 1\%$ error
- The field across the coil has higher error, but stresses are evaluated with a $\sim 5\%$ error

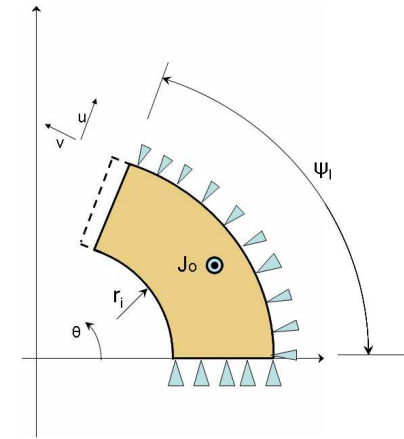
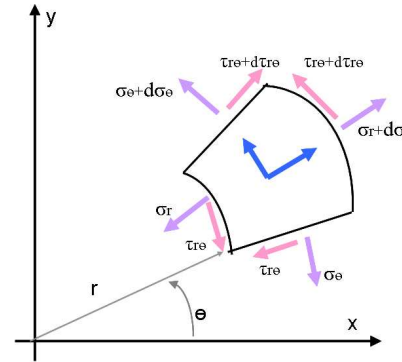
$$A_z(r, \theta) = \frac{4\mu_0 J}{\pi} \left\{ \frac{1}{4} r^2 \ln \left(\frac{r_i + w}{r} \right) \cos 2\theta \sin 2\phi_l + \sum_{n=6,10,14,\dots} \left[\frac{r^n}{n^2(n-2)} [r^{2-n} - (r_i + w)^{2-n}] \sin n\phi_l \cos n\theta \right] + \sum_{n=2,6,10,\dots} \left[\frac{r^{-n}}{n^2(n+2)} [r^{2+n} - r_i^{2+n}] \sin n\phi_l \cos n\theta \right] \right\}.$$

$$\vec{B} = \vec{\nabla} \times \vec{A} \quad \left\{ \begin{array}{l} B_\theta(r, \theta) = -\frac{\partial A_z}{\partial r} \\ B_r(r, \theta) = \frac{1}{r} \frac{\partial A_z}{\partial \theta} \end{array} \right.$$

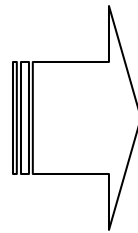


Mechanical model

- 2D plane strain
- Constraints on middle section and outer radius



- The shear in cylindrical coordinates is neglected



$$\left\{ \begin{aligned} \sigma_\theta(r, \theta) &= -J_0 (A_z(r, \theta) - A_z(r, \phi_l)) \\ \sigma_r(r, \theta) &= \frac{J_0}{r} \int_{r_i}^r \left[A_z(\bar{r}, \phi_l) - A_z(\bar{r}, \theta) - \frac{\partial(A_z)}{\partial \bar{r}} \bar{r} \right] d\bar{r} \end{aligned} \right.$$

Decoupled equations:
analytical solution

Mechanical model - Maximum Stress

$$\sigma_{\theta n}(r, \theta, w, r_i, \phi) := \left[\frac{\left(r^4 - r_i^4 + 4r^4 \cdot \ln\left(\frac{r_i + w}{r}\right) \right) \cdot (\sin(4\phi) + \sin(2\theta - 2\phi) - \sin(2\theta + 2\phi))}{32r^2} \right]$$

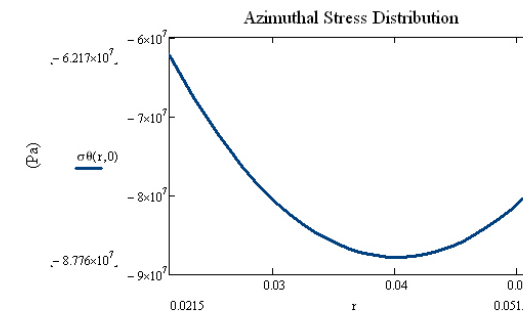
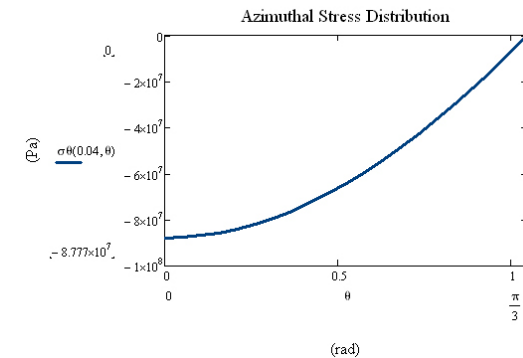
$$\sigma_{\theta n}(r, w, r_i, \phi) := \frac{1}{r} \int_{r_i}^r \frac{\left(y^4 - r_i^4 + 4y^4 \cdot \ln\left(\frac{r_i + w}{y}\right) \right) \cdot (\sin(4\phi) + \sin(2\theta - 2\phi) - \sin(2\theta + 2\phi))}{32y^2} dy - \frac{1}{r} \int_{r_i}^r \frac{\sin(2\phi) \cdot \left(r_i^4 - y^4 + 4y^4 \cdot \ln\left(\frac{r_i + w}{y}\right) \right)}{8y^2} dy$$

$$\left\{ \begin{array}{l} \frac{\partial \sigma_{\theta}}{\partial \theta} = -r f_{\theta} = -r J_0 B_r \\ B_r < 0 \end{array} \right. \Rightarrow \frac{\partial \sigma_{\theta}}{\partial \theta} > 0$$

Maximum abs σ_{θ}
in middle section

$|\sigma_{\theta}|_{max}$ from the roots of $\frac{\partial(A_z(r,0))}{\partial r}$

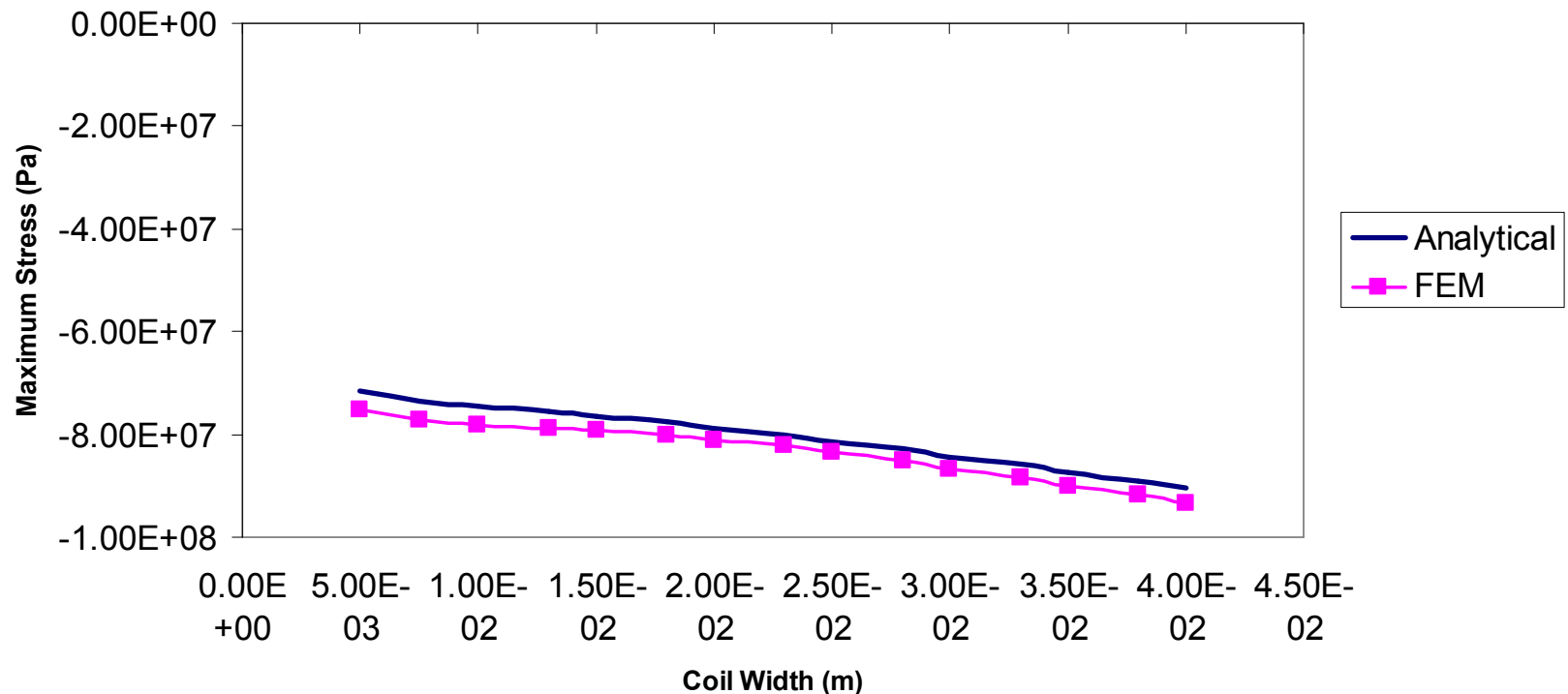
$$-4r^3 + 3(r_i + w) \cdot r^2 + r_i^3 = 0$$



Similarly, we proceed to find $|\sigma_r|_{max}$ for dipoles and quadrupoles

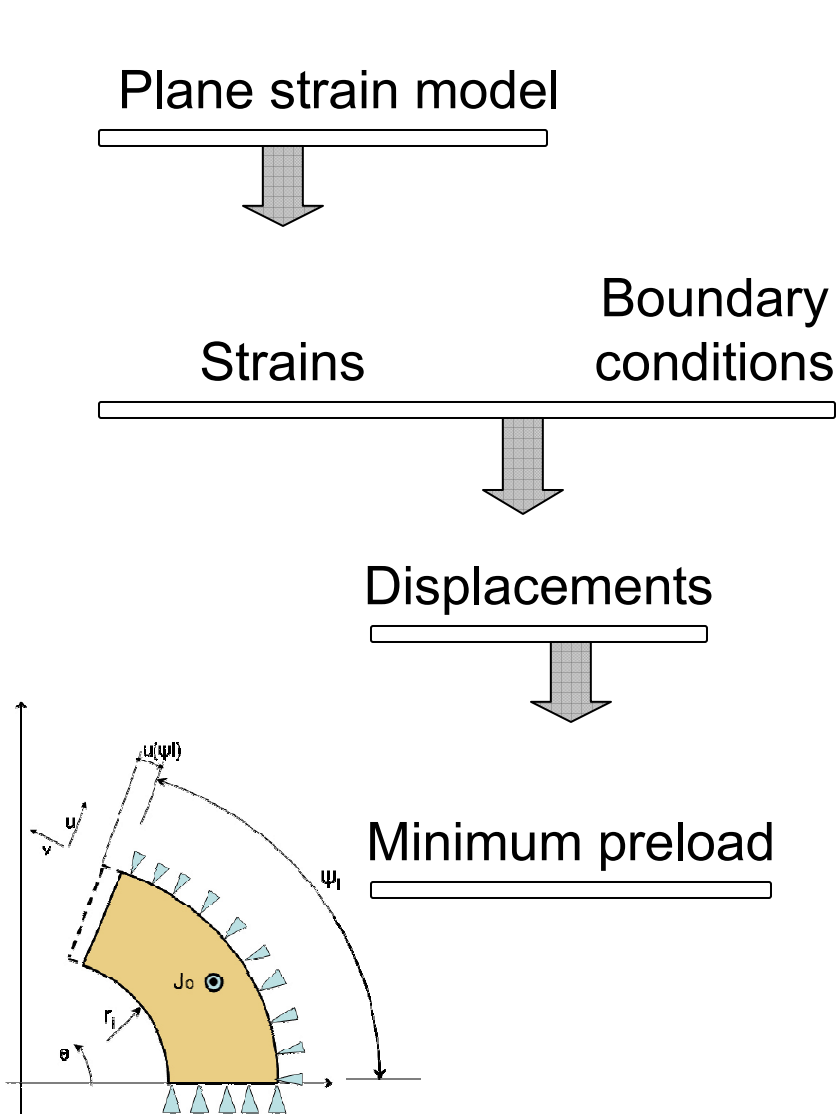
Mechanical model - accuracy

Discrepancy between Analytical Model and FEM



Discrepancy between analytical model and linear FEM model (with shear) is less than 5%

Mechanical model - Strains and displacements



$$\begin{bmatrix} \epsilon_{rr} \\ \epsilon_{\theta\theta} \\ \epsilon_{r\theta} \end{bmatrix} = \begin{bmatrix} \frac{1-\nu^2}{E} & -\frac{\nu(1+\nu)}{E} & 0 \\ -\frac{\nu(1+\nu)}{E} & \frac{1-\nu^2}{E} & 0 \\ 0 & 0 & \frac{1}{G} \end{bmatrix} \cdot \begin{bmatrix} \sigma_{rr} \\ \sigma_{\theta\theta} \\ \tau_{r\theta} \end{bmatrix}$$

$$\begin{cases} u(r = r_i + w, \theta) = 0 \\ v(r, 0) = 0 \end{cases}$$

$$\begin{cases} u(r, \theta) = \int_{r_i}^r \epsilon_r(\bar{r}, \theta) d\bar{r} - \int_{r_i}^{r_i+w} \epsilon(\bar{r}, \theta) d\bar{r} \\ v(r, \theta) = \int_0^\theta \epsilon_\theta(r, \bar{\theta}) r d\bar{\theta} - \int_0^\theta u(r, \bar{\theta}) d\bar{\theta} \end{cases}$$

$$\Delta_{min} = \max_r [v(r, \varphi_l)]$$

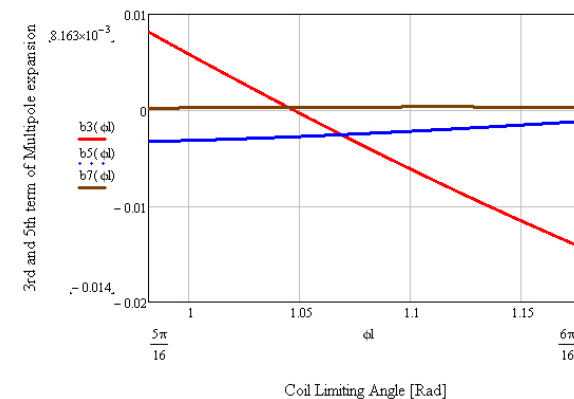
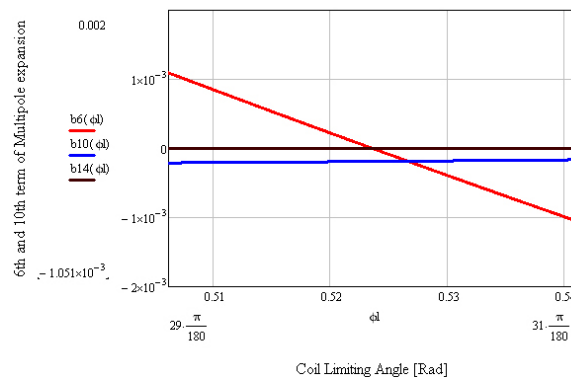
Field Quality

- The magnetic field can be expressed in its multipole expansion terms

$$B_{\theta}(r, \theta) = B_{ref} \sum_{n=1}^{\infty} \left(\frac{r}{r_0}\right)^{n-1} [b_n \cos n\theta + a_n \sin n\theta]$$

$$B_r(r, \theta) = B_{ref} \sum_{n=1}^{\infty} \left(\frac{r}{r_0}\right)^{n-1} [-a_n \cos n\theta + b_n \sin n\theta]$$

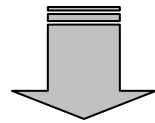
- Requirements on FQ usually ask field harmonics other than the principal to be $<10^{-4}$
- Such field cannot be obtained with a single layer layout



- We thus require in the model multipole terms's variations to be $<10^{-4}$

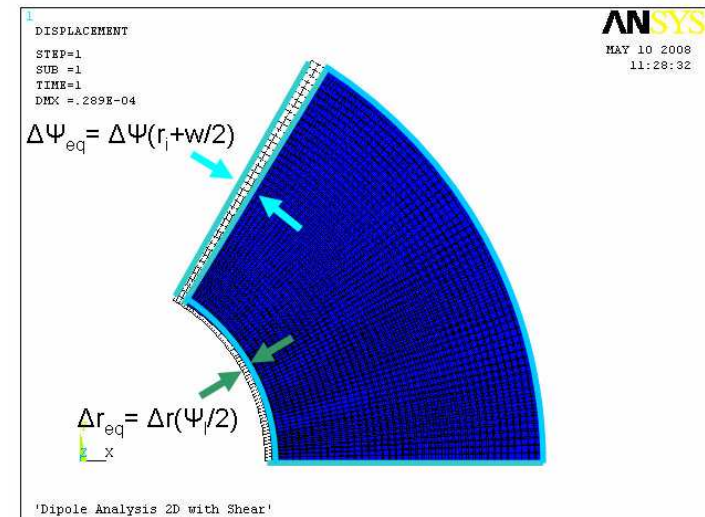
Loss of field quality

- 1) Variations in the shape of the coil
 - The deformed coil is approximated as a circular sector
 - The coil is not preloaded



$$B_{ref} = -\frac{r_i}{4} \ln \left(\frac{r_i + w}{r_i} \right) \sin 2\phi_l$$

$$b_n = \frac{[(r_i + w)^{2-n} - r_i^{2-n}]}{n(n-2)} \frac{\left(\frac{r_i}{2}\right)^{n-1}}{B_{ref}} \sin(n\phi_l)$$



Loss of field quality

2) Internal redistribution of the current density

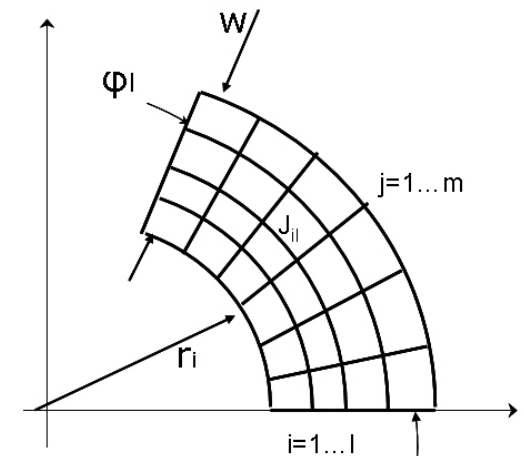
- The current density is proportional to the conductor density

$$\frac{\partial A}{\partial A_0} = 1 + \epsilon_r + \epsilon_\theta \quad \Rightarrow \quad J(r, \theta) = \frac{J_0}{1 + \epsilon_r + \epsilon_\theta}$$

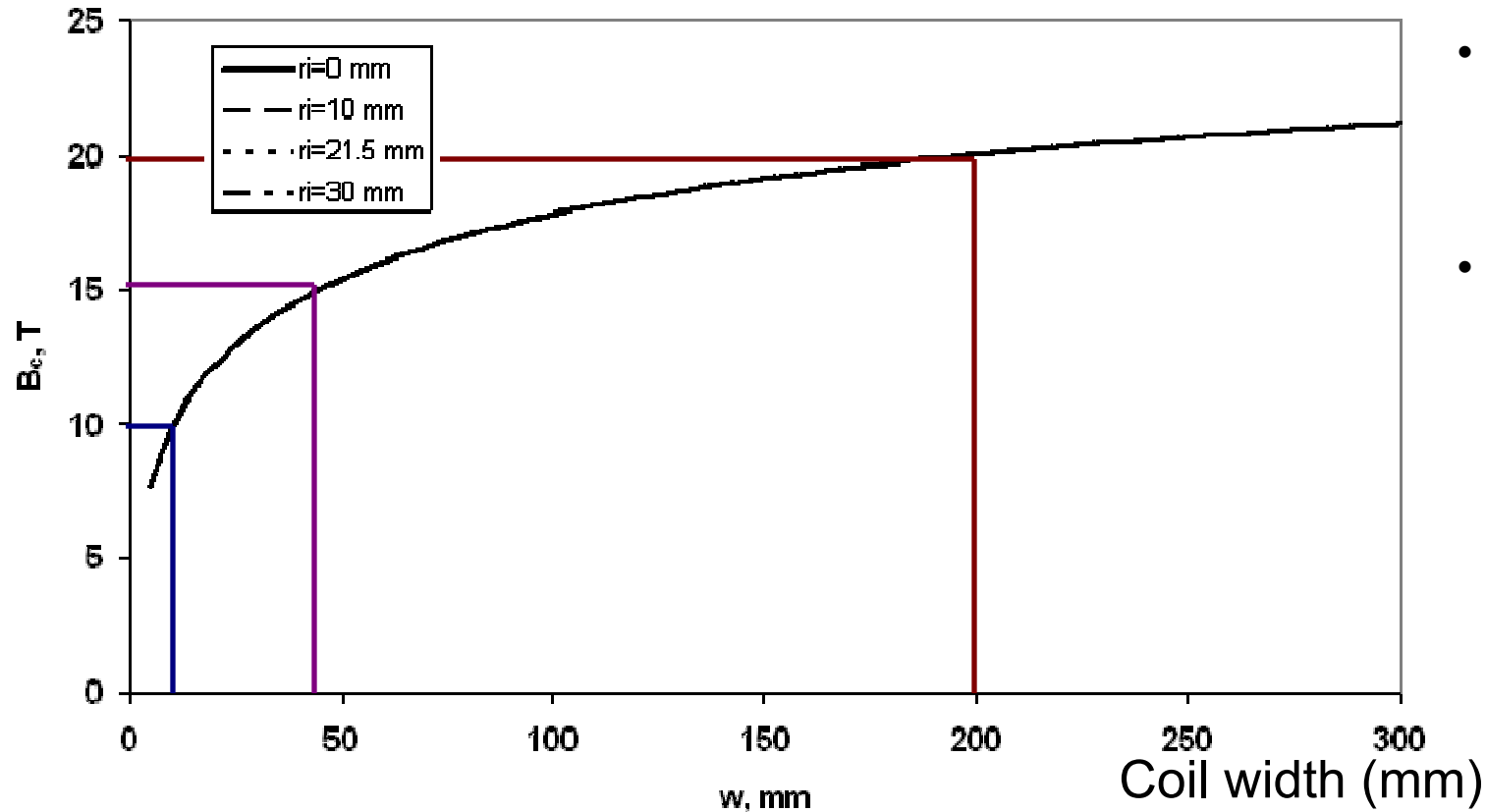
- Discretization of the coil sector

$$B_{ref} = - \sum_{i=1}^l \sum_{j=1}^m \left[\frac{2\mu_0 J \left(r_i + \frac{w}{l} \left(i - \frac{1}{2} \right), \frac{\phi_l}{m} \left(j - \frac{1}{2} \right) \right)}{\pi} \cdot \frac{w}{l} \left[\sin \left(\frac{\phi_l}{m} j \right) - \sin \left(\frac{\phi_l}{m} (j - 1) \right) \right] \right]$$

$$b_n = \frac{1}{B_{ref}} \left(\frac{r_i}{2} \right)^{n-1} \sum_{i=1}^l \sum_{j=1}^m \left[\frac{2\mu_0 J \left(r_i + \frac{w}{l} \left(i - \frac{1}{2} \right), \frac{\phi_l}{m} \left(j - \frac{1}{2} \right) \right)}{\pi} \frac{1}{n(n-2)} \cdot \left[\left[r_i + \frac{w}{l} (i-1) \right]^{2-n} - \left[r_i + \frac{w}{l} i \right]^{2-n} \right] \cdot \left[\sin \left(\frac{n\phi_l}{m} j \right) - \sin \left(\frac{n\phi_l}{m} (j-1) \right) \right] \right]$$



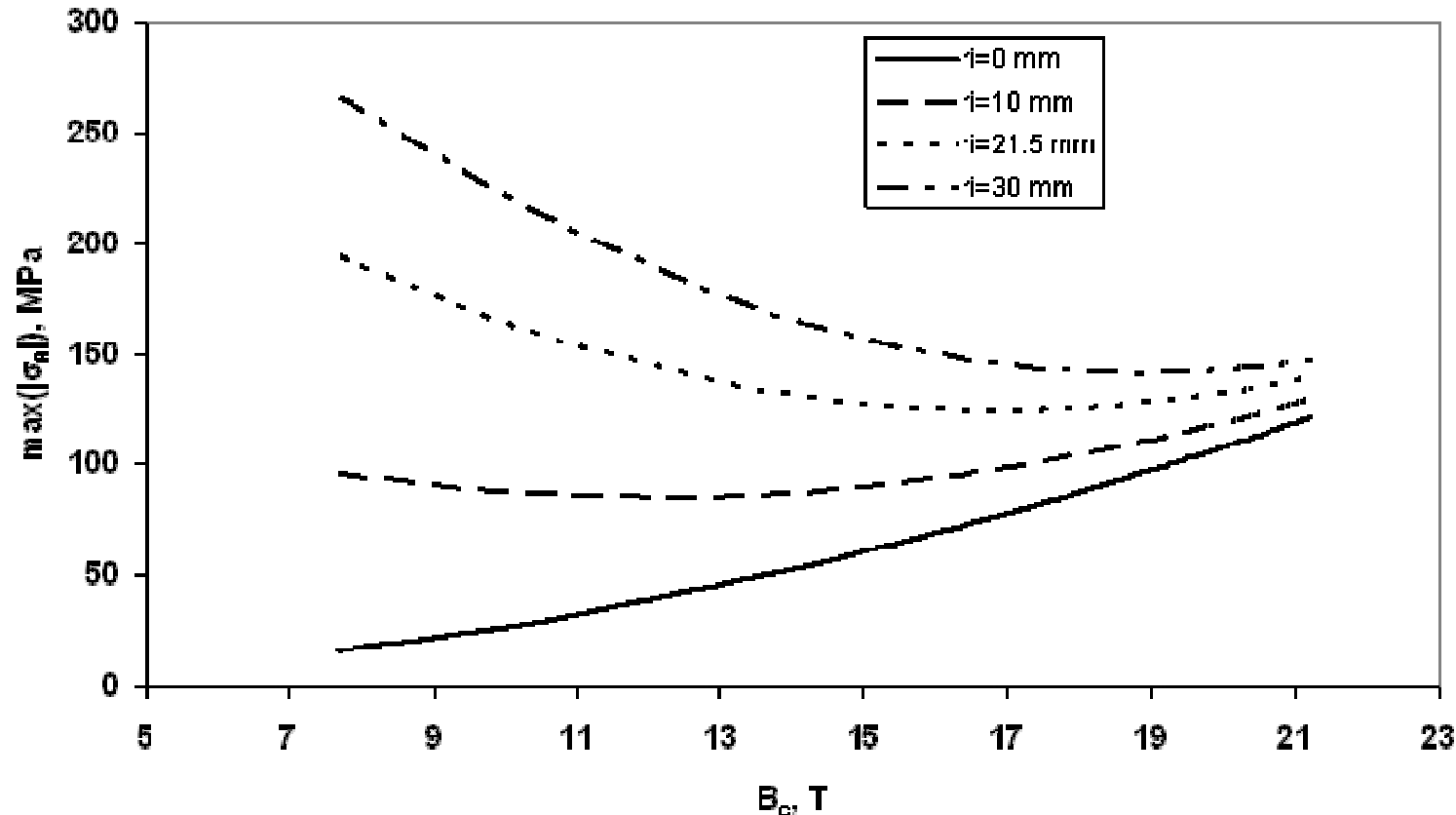
Magnet performance - Field intensity in dipoles



- $r_i = 0$,
 $r_i = 10$ mm,
 $r_i = 21.5$ mm,
 $r_i = 30$ mm
- $0 < w < 300$
mm

- The maximum field is independent of the bore diameter: $B_c = B_c(w)$
- At 4.2 K, if $w = 10$ mm generates 10 T, 45 mm are needed for 15 T
- A coil width $w = 200$ mm of this cable is needed to reach 20 T
- A twentyfold increase in coil area is required from 15 T to 20 T

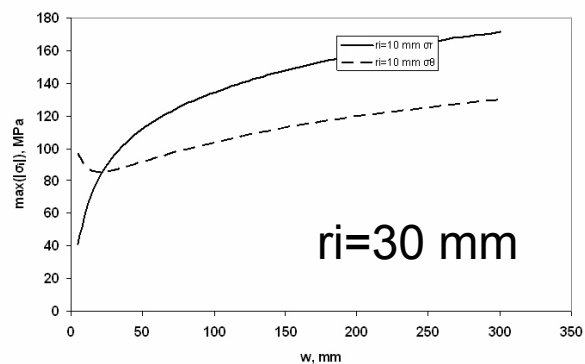
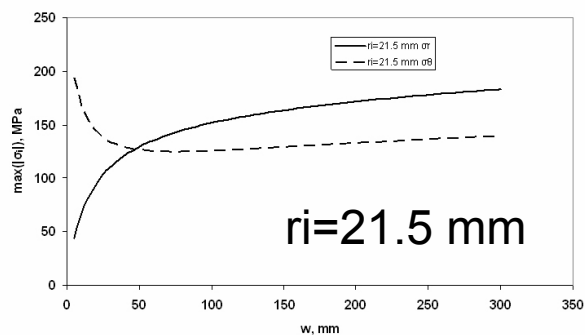
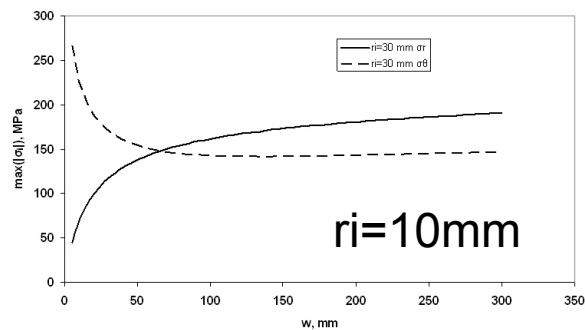
Magnet performance - σ_θ in dipoles



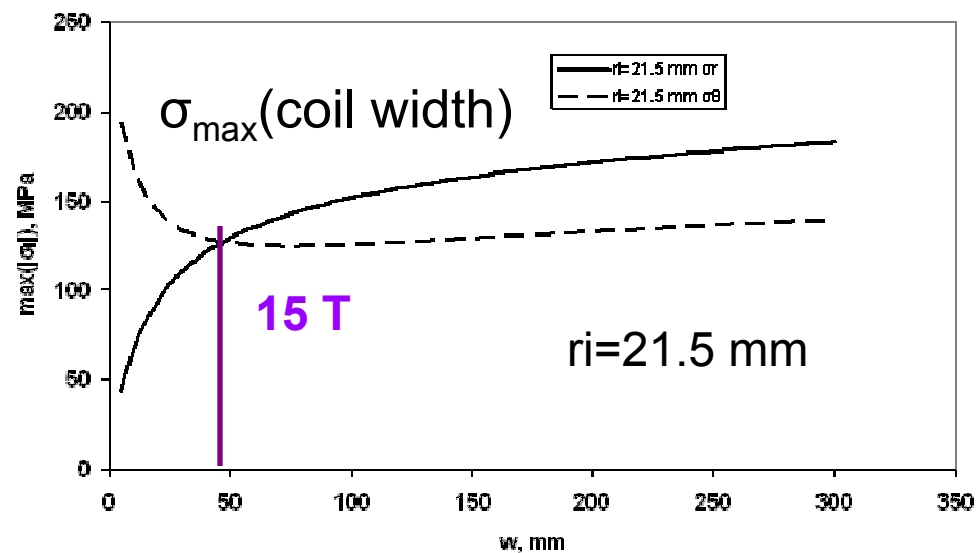
- As done by Caspi05, we look at the axial stress
- A constant current density replaces a $\cos\theta$ distribution

- The zero bore solution is the minimum for any r_i at that B_c
- For larger r_i , σ_θ decreases as B_c increases, due to lower efficiency

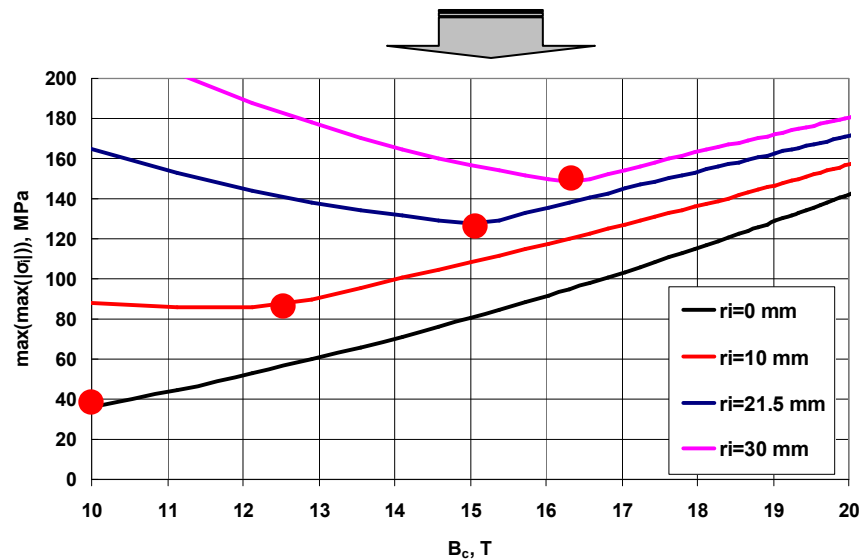
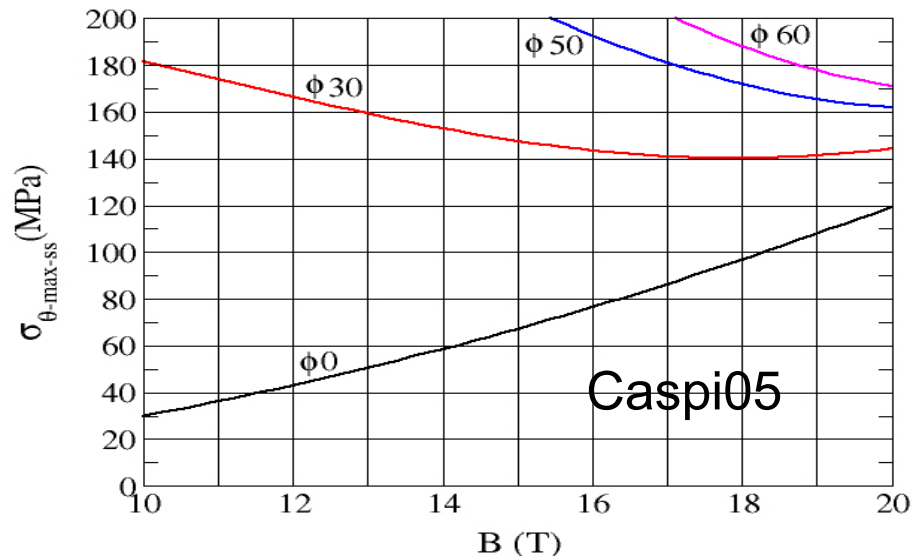
Magnet performance - σ_r in dipoles



- For small widths, σ_θ prevails over σ_r since the integration path is longer
- For larger widths, σ_r tends to prevail, and should therefore be taken into account
- σ_r should be included in parametric analyses
- Multiaxiality should be addressed ($\sigma_r = \sigma_\theta$ at 15T)

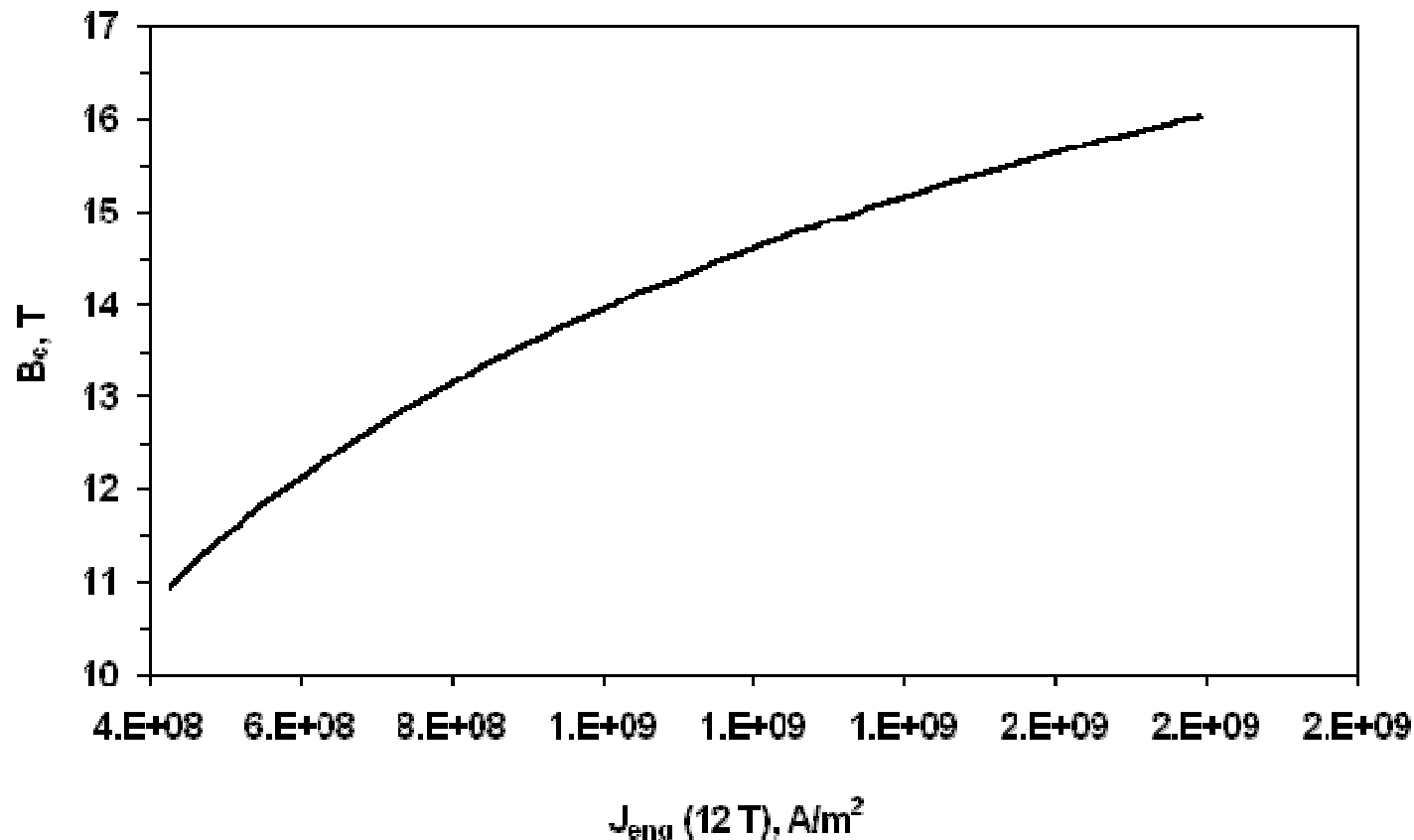


Magnet performance - σ_{\max} in dipoles



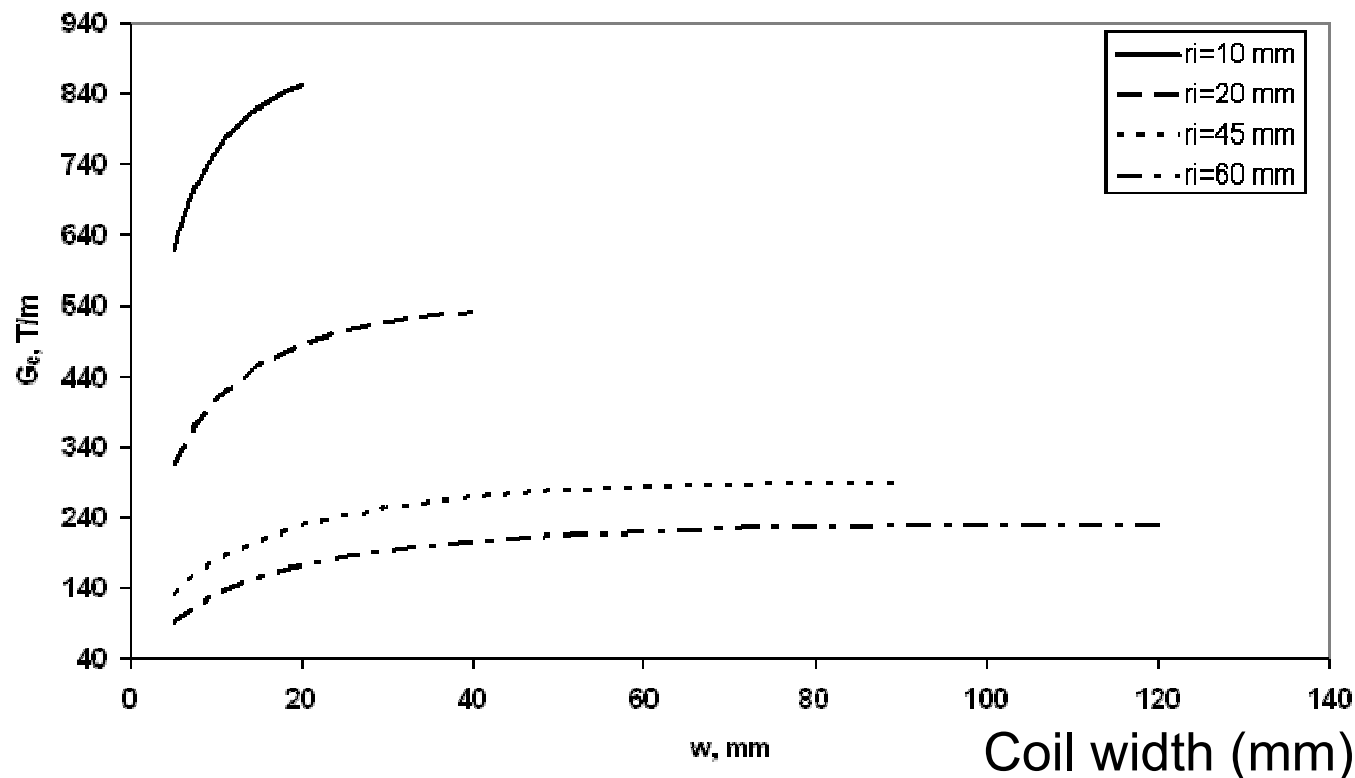
- At **12.5 T** $\sigma_r > \sigma_\theta$ for $ri=10$ mm
- A **20 T dipole** with $ri=21.5$ mm has $\sigma_r=170$ MPa and $\sigma_\theta=133$ MPa
- A 18 T dipole requires a coil 105 mm thick, $\sigma_r=153$ MPa and $\sigma_\theta=126$ MPa
- At very high fields the effect of bore diameter on maximum stress is minor

Magnet performance - cable properties



- As the field gets closer to Nb_3Sn critical field, a better performing cable brings smaller improvements

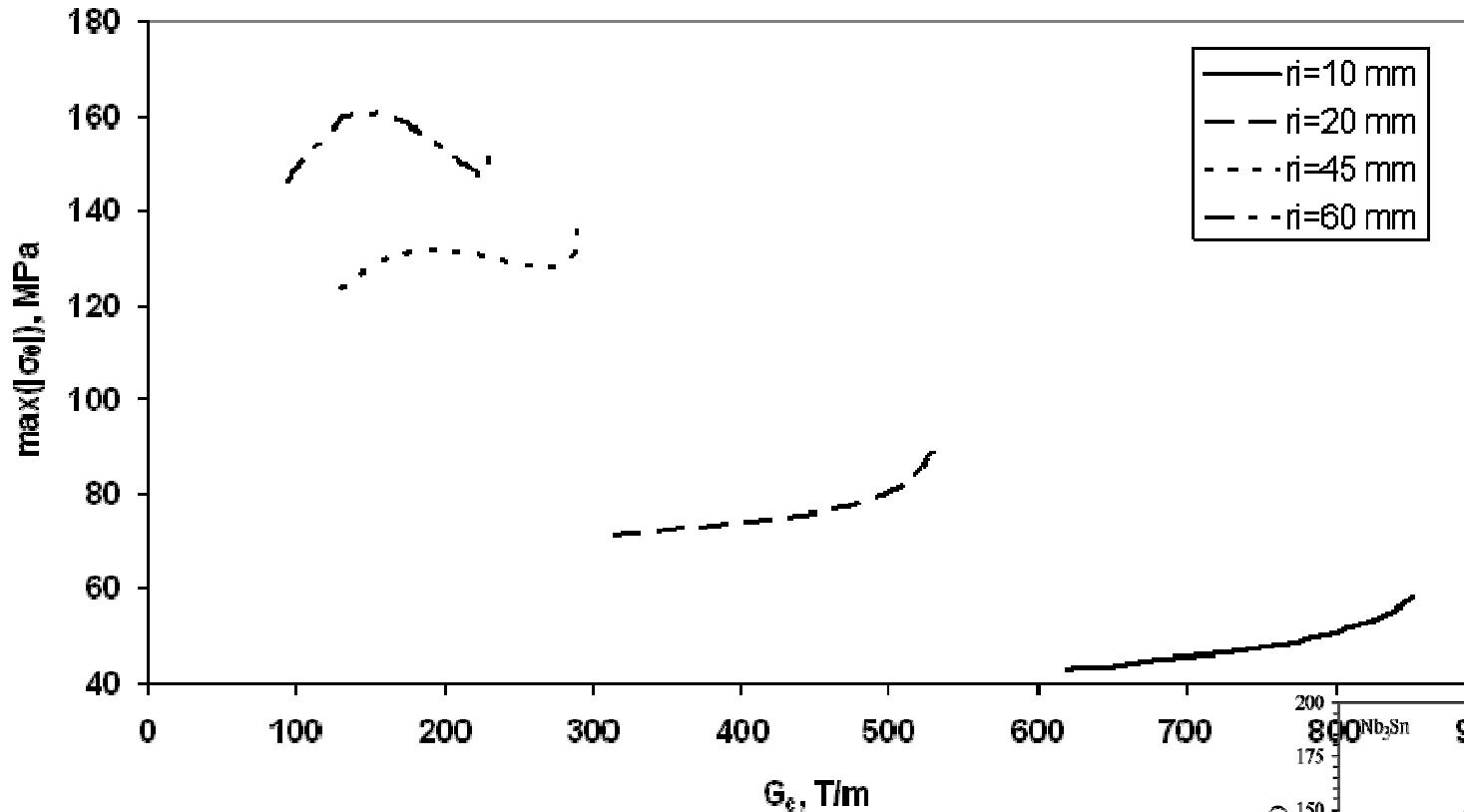
Magnet performance - G_c in quadrupoles



- $r_i=10$ mm,
 $r_i=20$ mm,
 $r_i=45$ mm,
 $r_i=60$ mm
- $5 < w < 2 r_i$
mm

- Larger bores have smaller gradients, but $G_c r_i$ improves at larger bores
- Adding material doesn't always improve the gradient: $G_c \sim j \log(w)$ while $B_{max} \sim j w \log(w)$

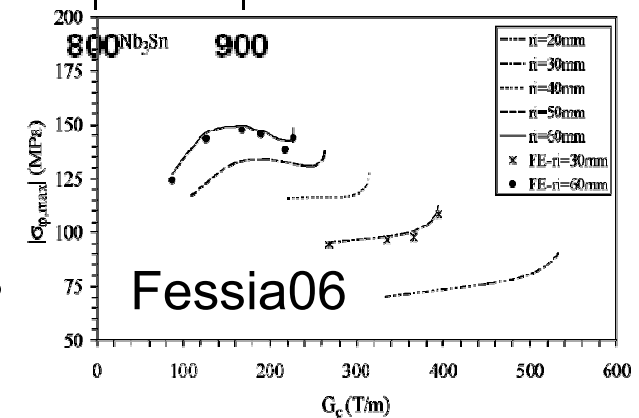
Magnet performance - σ_θ in quadrupoles



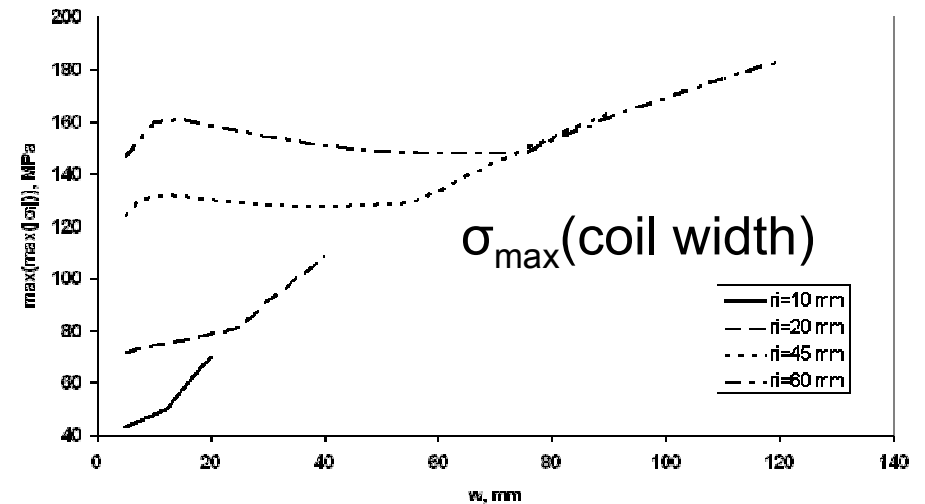
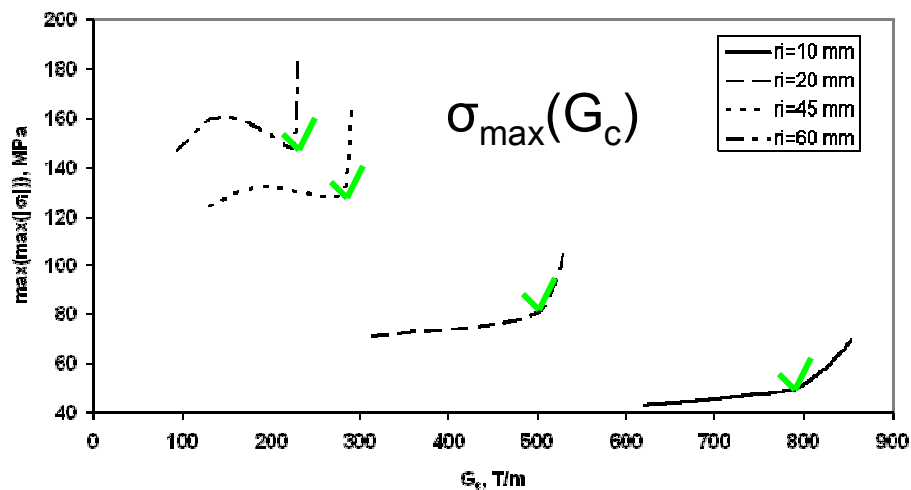
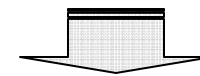
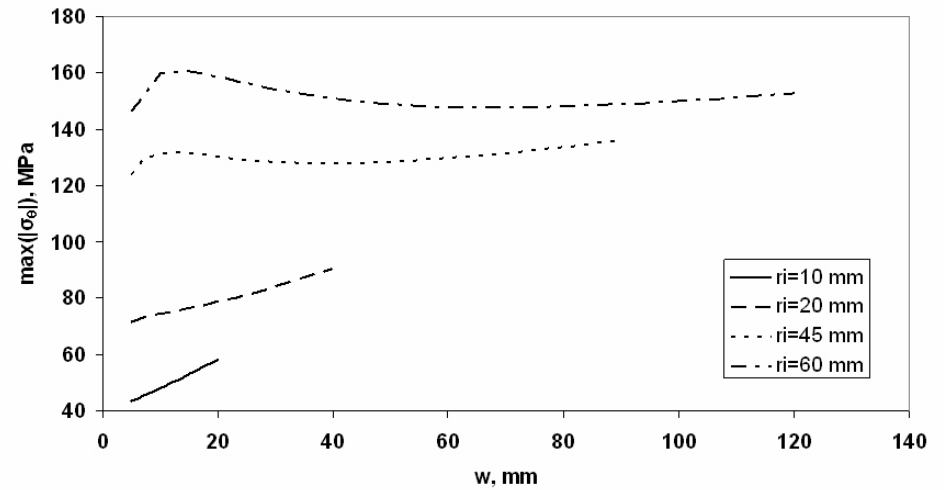
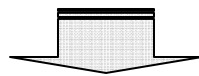
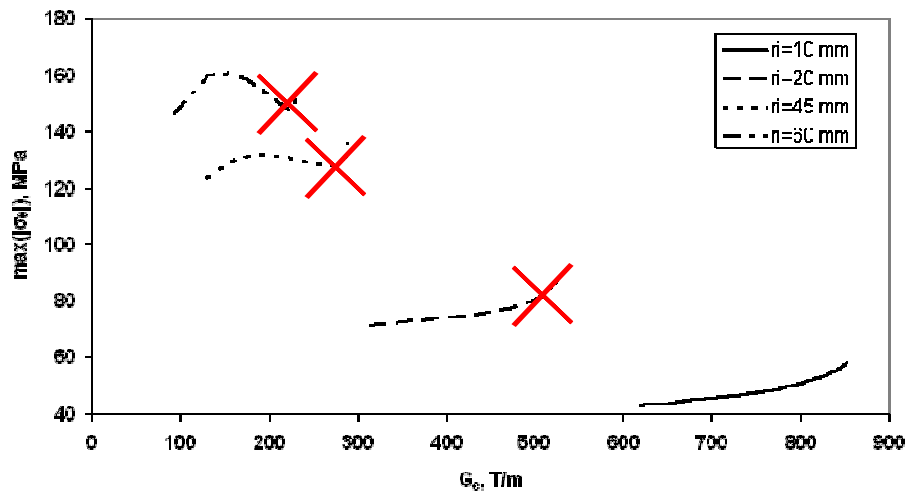
- As done by Fessia07, we only plot the aximuthal stress
- The trends are reproduced



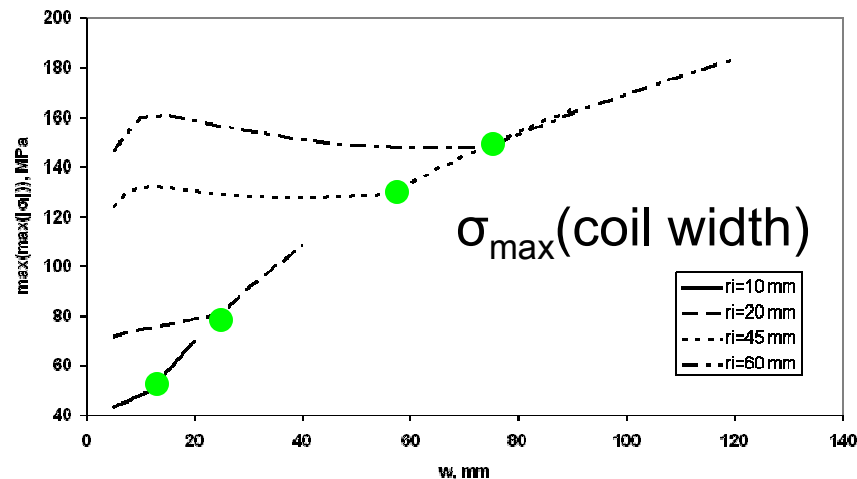
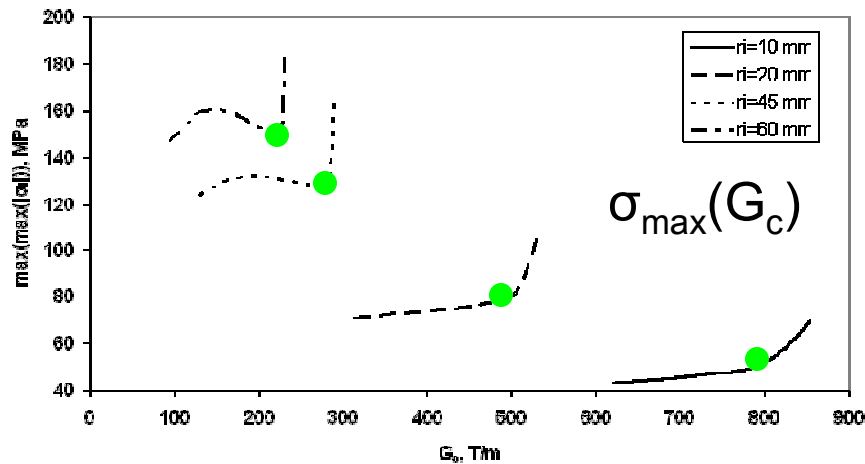
- $\sigma_\theta > 150$ MPa for $r_i=60$ mm
- σ_θ can decrease with G_c , as the increase in w is much larger than the one in G_c



Magnet performance - σ_r in quadrupoles

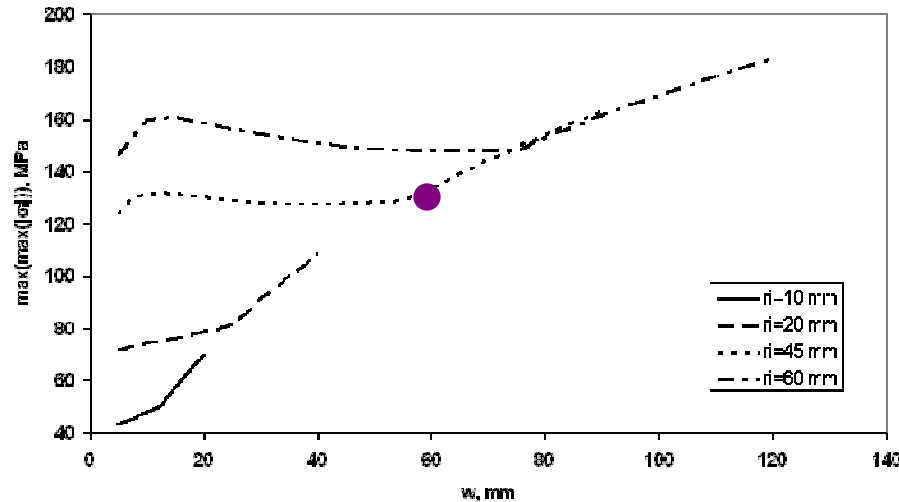


Magnet performance - σ_{\max} in quadrupoles

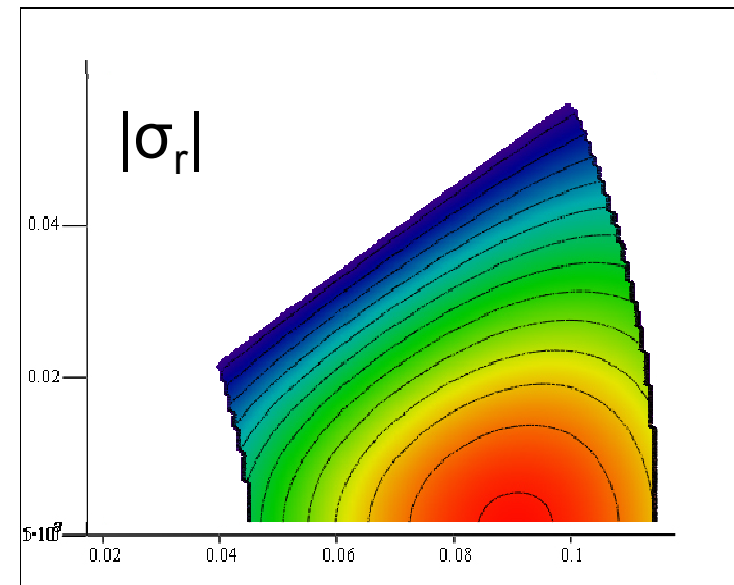
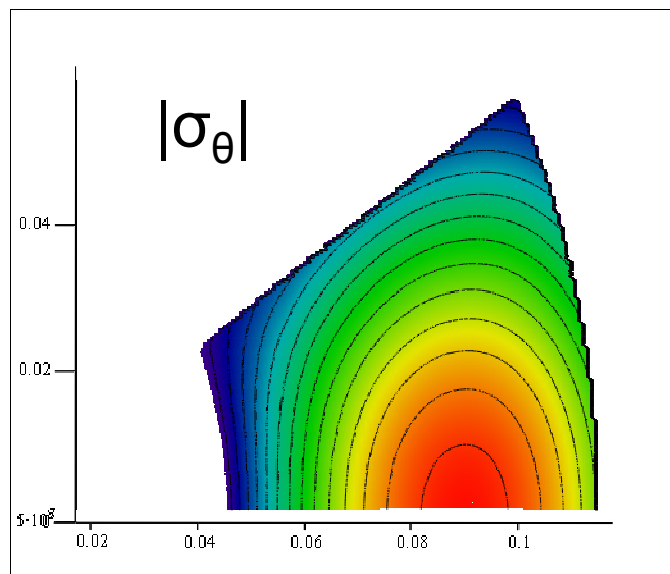


- For small widths, σ_{θ} prevails over σ_r since the integration path is longer
- For larger widths, σ_r tends to prevail, and should therefore taken into account
- We should address multiaxiality
- The 150MPa limit is only exceeded for very large apertures
- σ_r has a strong dependence on w , and is independent of r_i
- A good design choice for maximum performance is the geometry that has $\sigma_{\theta} = \sigma_{\theta r}$

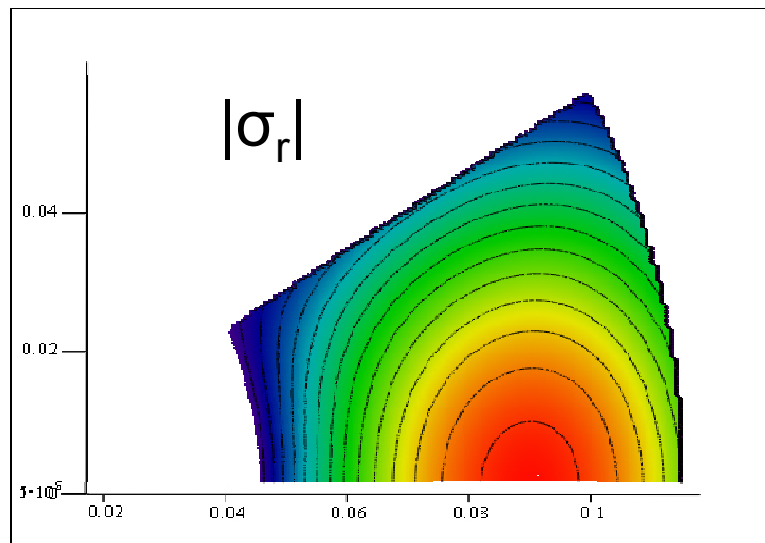
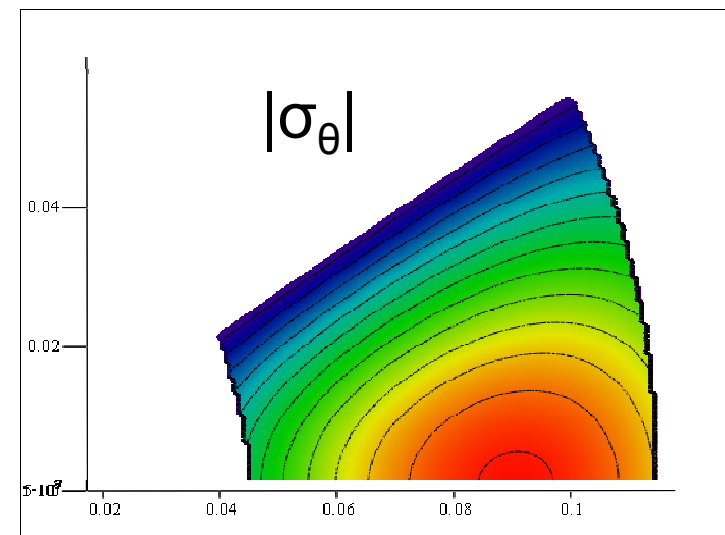
Multiaxiality of the stress tensor



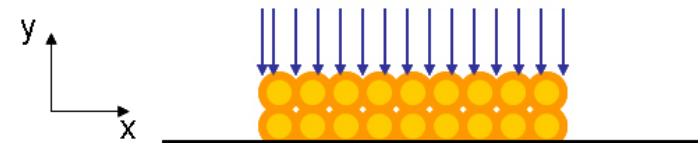
- We chose a quadrupole geometry with a strong multiaxiality
- We wanted to evaluate the importance of multiaxiality in the coil performance



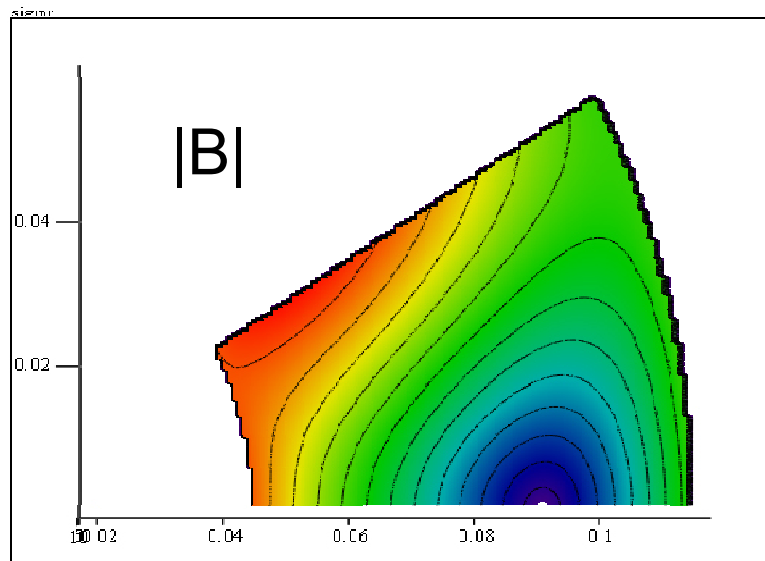
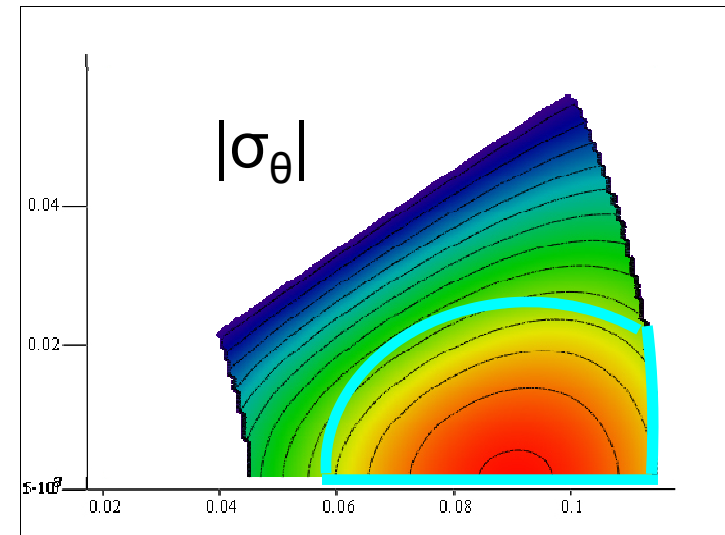
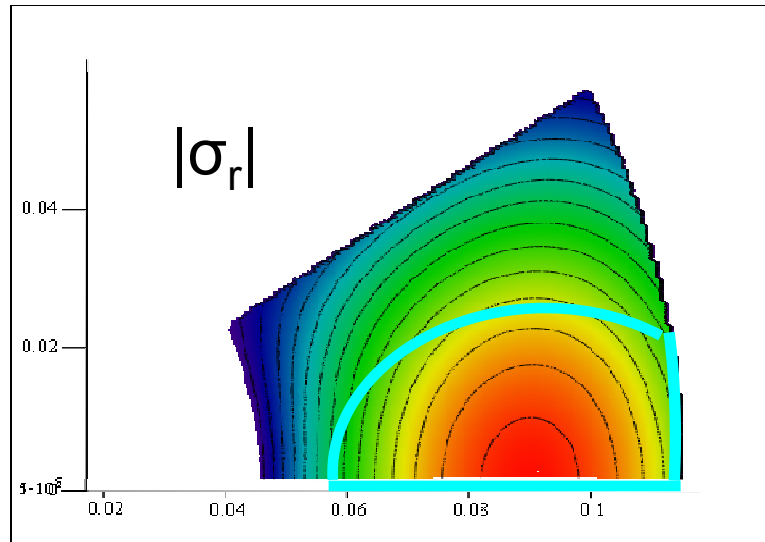
Multiaxiality of the stress tensor

sign_rsign_θ

- Multiaxiality is located in the bottom-right part of the coil.
- On the top and left edges the stress tensor is uniaxial



Multiaxiality of the stress tensor

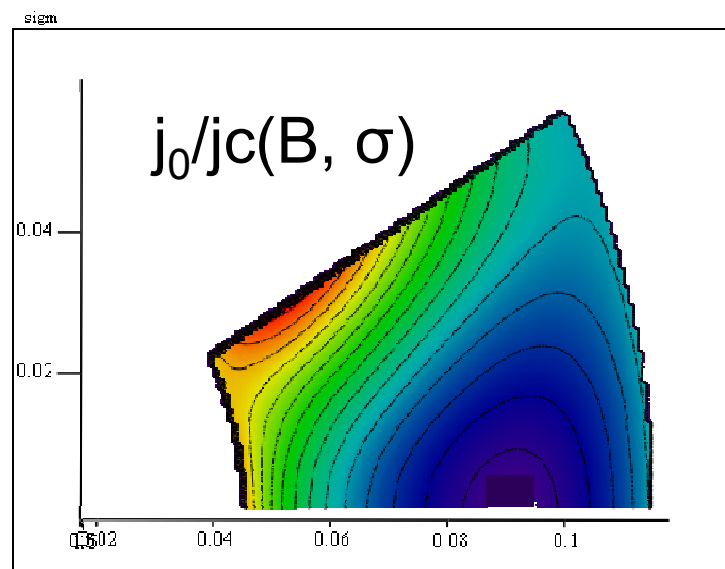
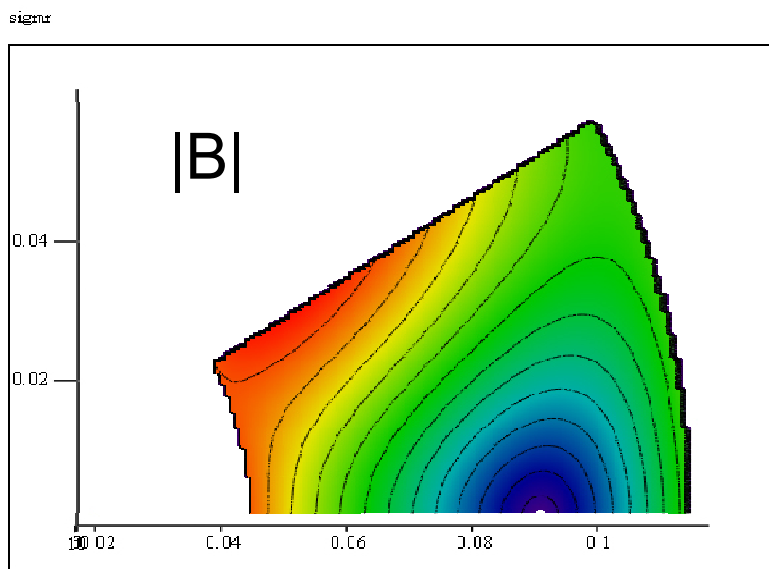
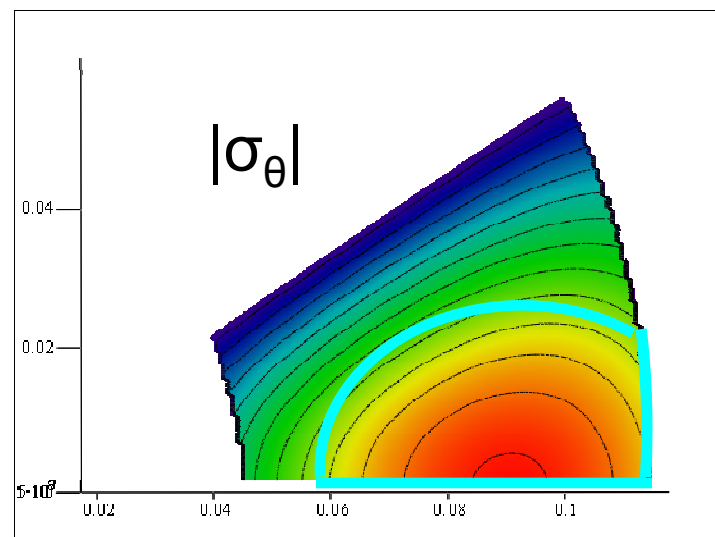
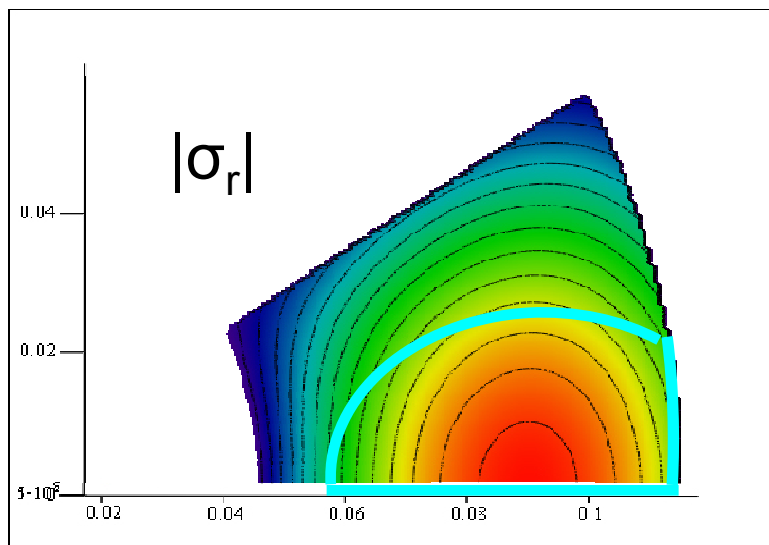


sign

- The highest field area is located along $r=r_i$ and $\theta=\varphi_i$
- Multiaxiality doesn't play a primary role in single-layer quadrupole quench

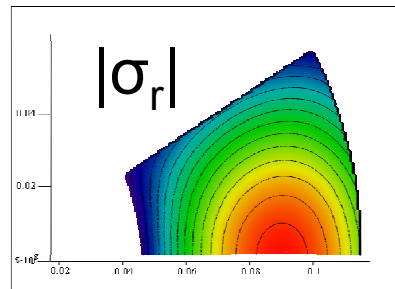
BBB

Multiaxiality of the stress tensor

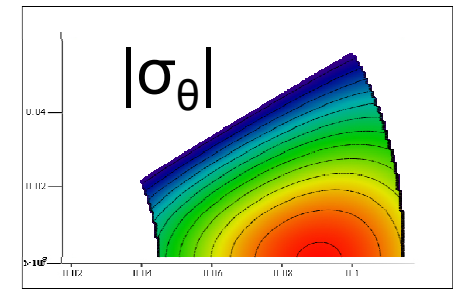


Multiaxiality of the stress tensor

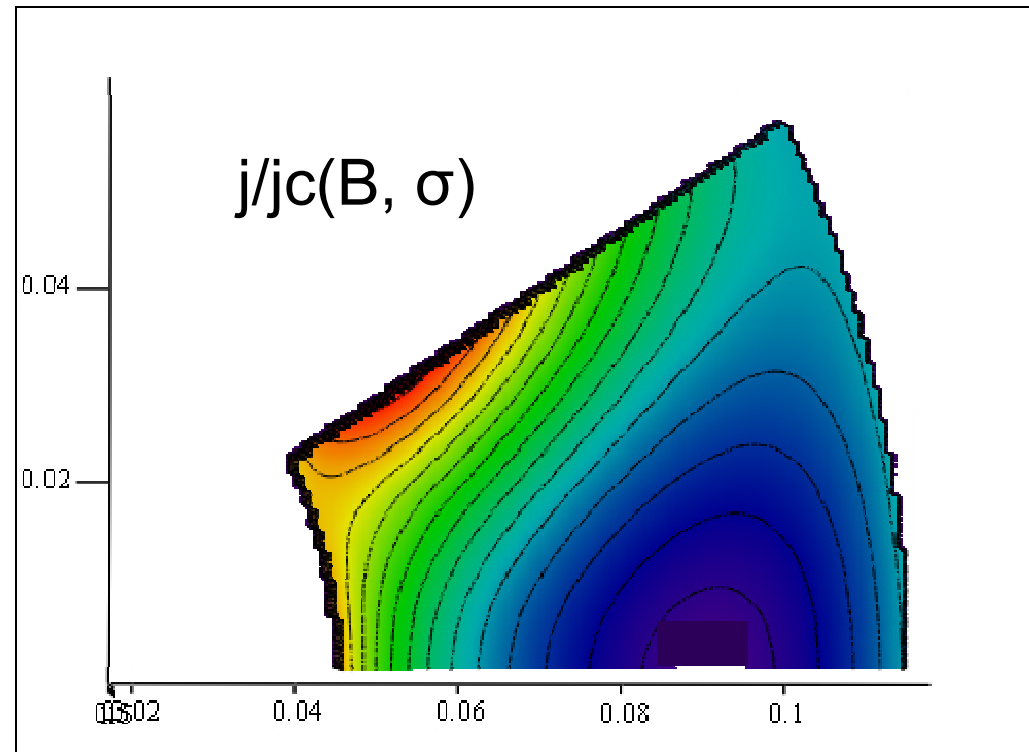
- The *multiaxiality* of the stress tensor can be *neglected* in magnet performance analysis
- The *quench occurs in a zone where σ_θ is negligible*, it has thus a secondary effect on the degradation of the cable properties
- For this geometry, $\sigma_\theta=130$ MPa, $\sigma_r=145$ MPa
- In a conservative analysis, we can consider that the *critical point is subject to $\sigma_{r,max}$* , which looks more appropriate than σ_θ



sigma



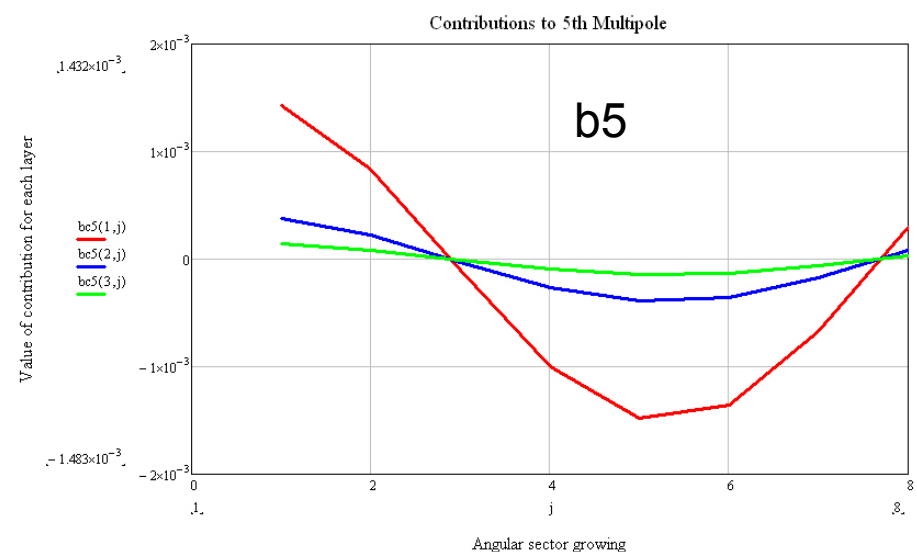
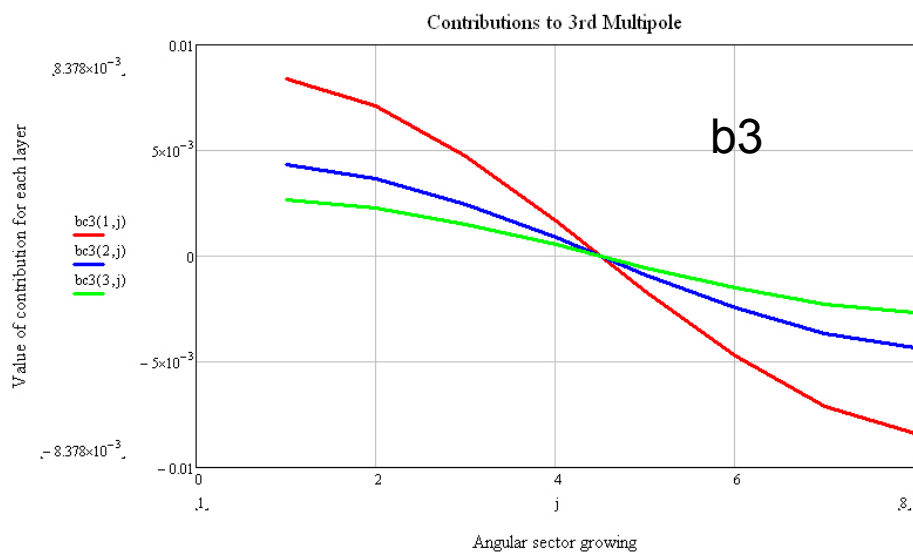
sigma



C

Field quality – multipole coefficients

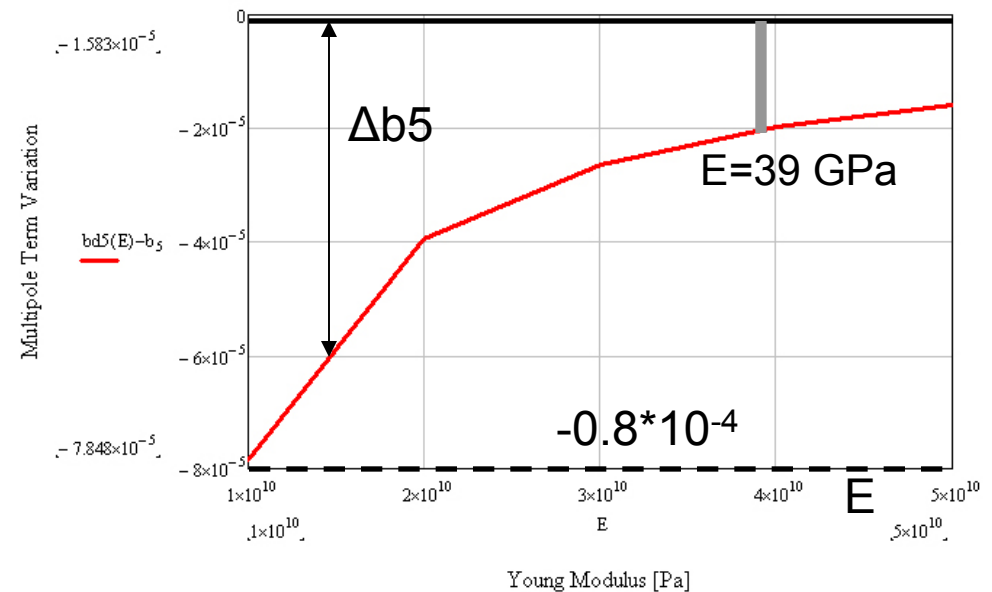
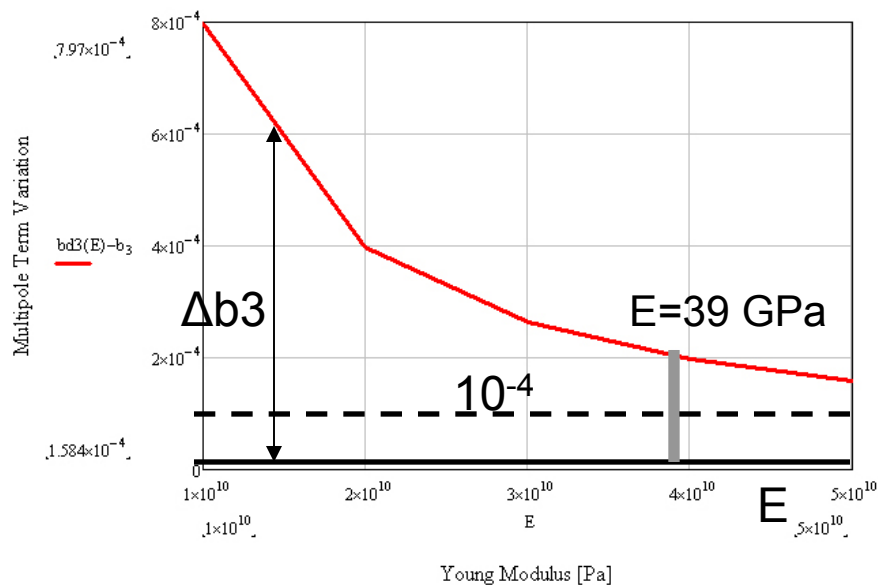
Contribution of dipole parts to residual multipole coefficients. Integral must go to 0.



- The plot of b_3 accounts for the fact that a coil that is compressed in the azimuthal direction shows a positive b_3
- This information can be used as a guide to design coil geometries, as it indicated where to add/remove conductor in order to cancel residual multipole coefficients

Field quality – unpreloaded coil

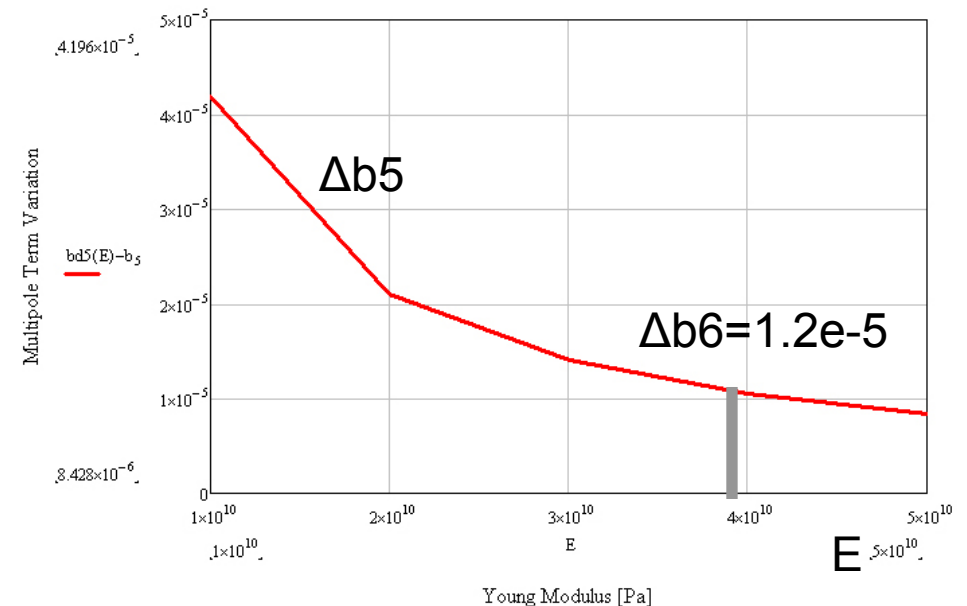
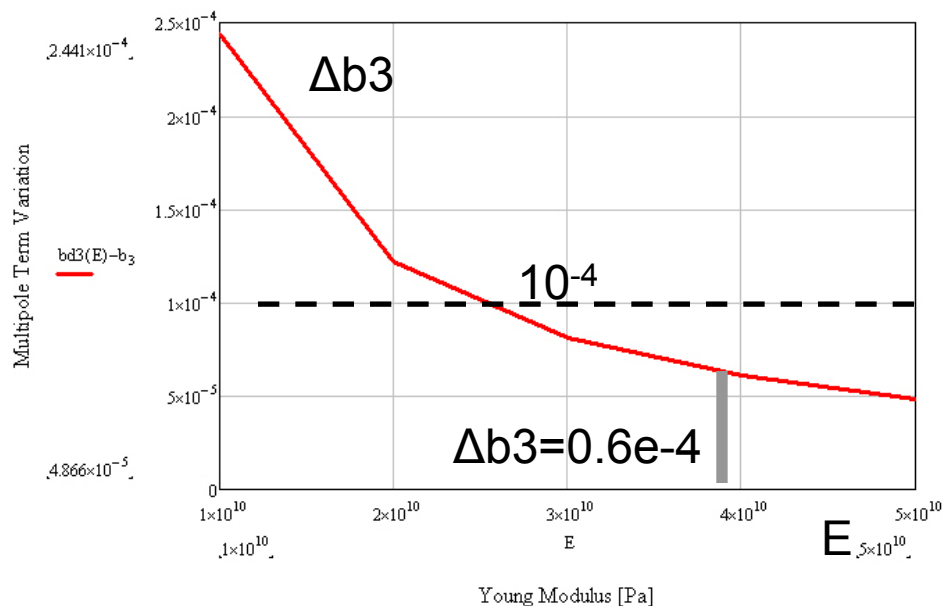
Multipole terms variation due to the coil deformation induced by the Lorentz force.
 Dipole $r_i=21.5$ mm, $w=20$ mm



- For $E=39$ GPa (neglecting plasticity) Δb_3 is twice the maximum allowed value, meaning a preload of the coil is necessary
- Δb_5 is always below the 10^{-4} limit

Field quality - Redistribution of J_c

Multipole terms variation due to the internal redistribution of J_c . Dipole $r_i=21.5$ mm, $w=20$ mm



- Current density variation does not cause multipole terms' variations greater than $1e-4$, both for dipoles and quadrupoles
- The preload reduces $\Delta b3$ to 20% of value with no preload
- Higher order terms show variations within requirements

Outline

I. A Parametric Model for Electromechanical Effects in HFMs

- Linear
- Analytic solutions
- Limits of HFMs

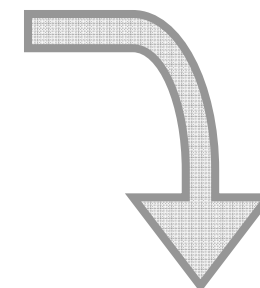


Results suggest the need of

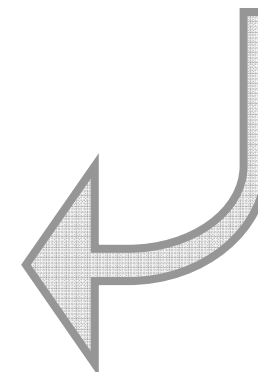
II. An experiment for equivalent stress in HFMs

III. A FEM Elastoplastic Model

- Accuracy of parametric model
- Non-linear phenomena



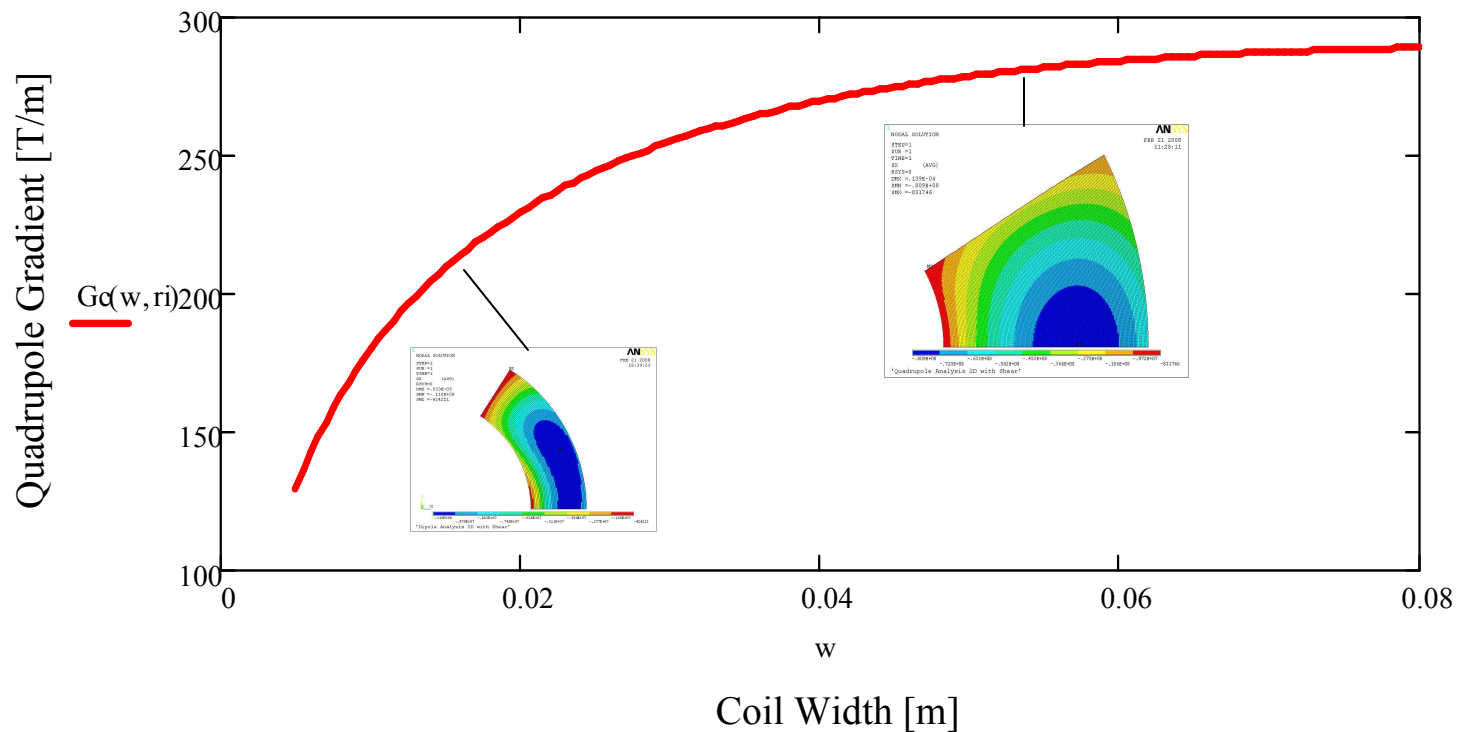
The P.M. was checked and integrated with



II. Equivalent stress in HFMs - Outline

- Introduction
 - Design trends in HFMs
 - Stress sensitivity of SC cables
- Multiaxiality
- Candidates ε_{eq}
- Data interpretation

Trends in HFMs



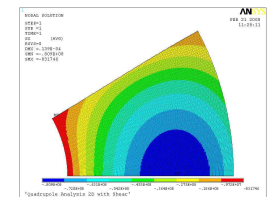
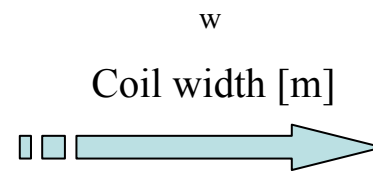
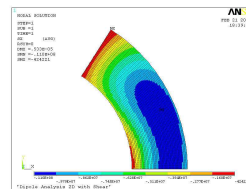
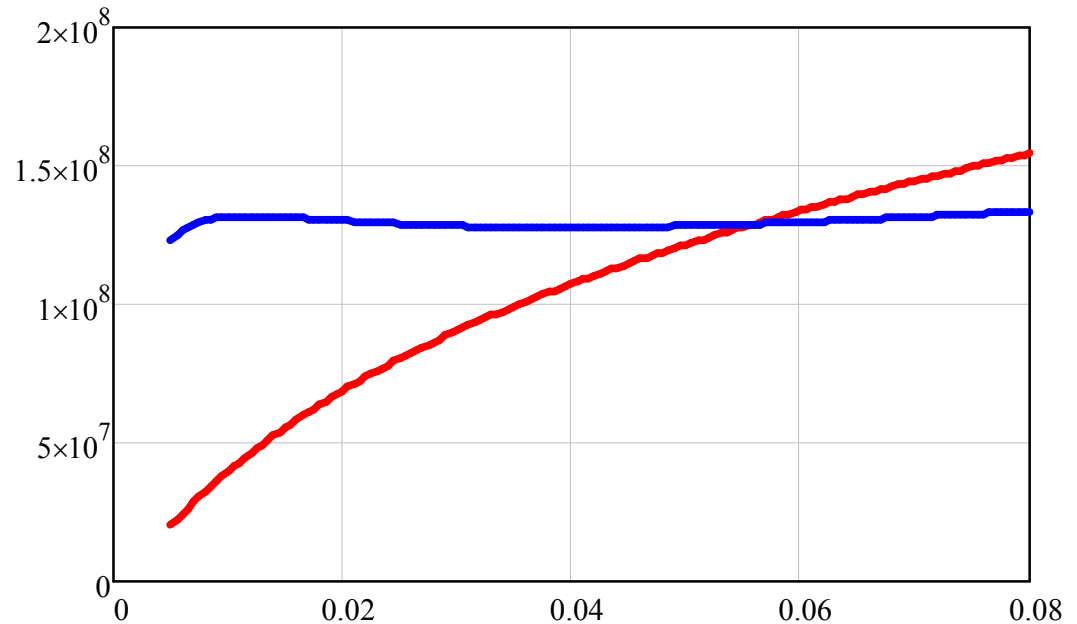
$$A_{zn}(r, \theta, w, r_i, \phi) := \left[\frac{2}{r} \cdot \ln\left(\frac{r_i + w}{r}\right) \cdot \cos(2 \cdot \theta) \cdot \sin(2 \cdot \phi) + \sum_{n=0}^{n_{\max}} \left[\frac{1}{(4 \cdot n + 2)^2} \cdot \frac{1}{r^{4 \cdot n + 2}} \cdot \left[\frac{r^{4 \cdot n + 4} - r_i^{(4 \cdot n + 4)}}{4 \cdot n + 4} \right] \cdot \cos[(4 \cdot n + 2) \cdot \theta] \cdot \sin[(4 \cdot n + 2) \cdot \phi] \right] \right]$$

Trends in HFMs

Coil Max Stress [Pa]

— $\sigma_r(\text{root}(\text{dorn}(p, w, r_i, \phi), p), 0, w, r_i, \phi)$

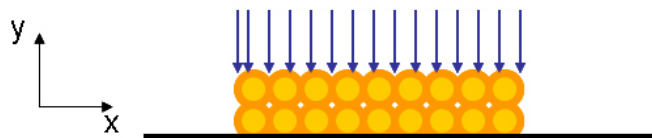
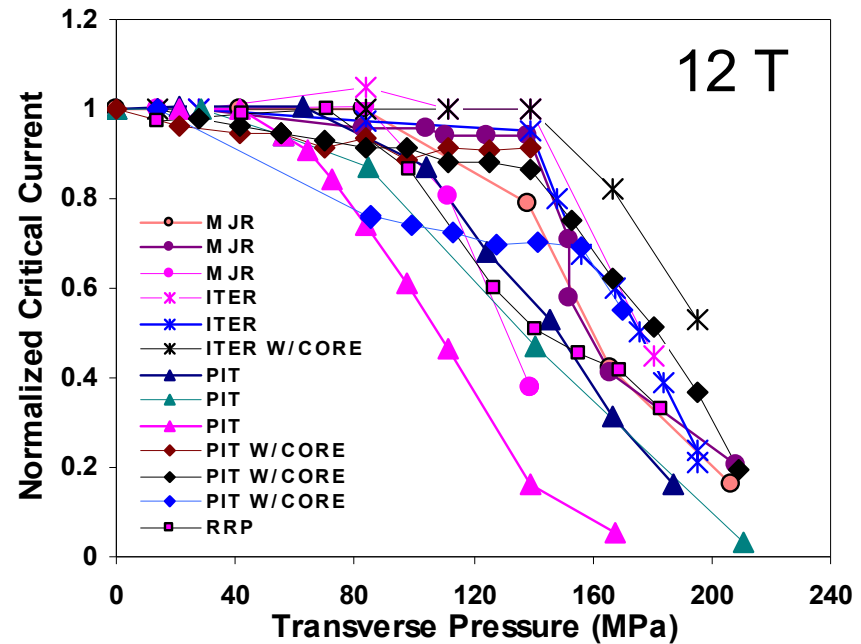
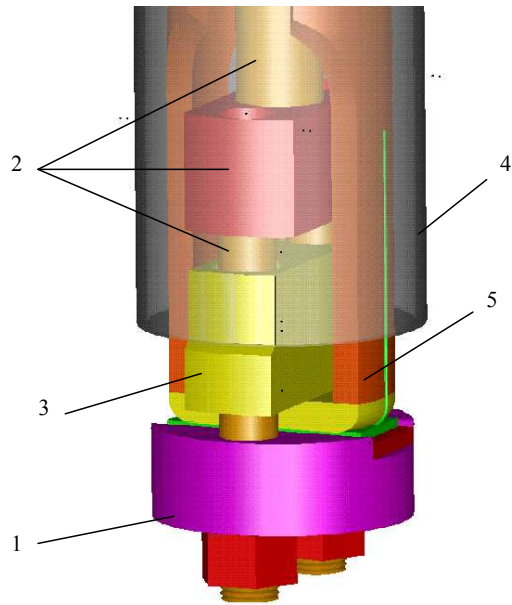
— $\sigma_\theta\left(\text{root}\left(4 \cdot x \cdot \ln\left(\frac{r_i+w}{x}\right) + \frac{r_i^4}{x^3} - x, x\right), 0, w, r_i, \phi\right)$



$$\sigma_{\theta n}(r, \theta, w, r_i, \phi) := - \frac{\left[r^4 - r_i^4 + 4 \cdot r^4 \cdot \ln\left(\frac{r_i+w}{r}\right) \right] \cdot (\sin(4 \cdot \phi) + \sin(2 \cdot \theta - 2 \cdot \phi) - \sin(2 \cdot \theta + 2 \cdot \phi))}{32 \cdot r^2}$$

$$\sigma_{rn}(r, \theta, w, r_i, \phi) := \frac{1}{r} \int_{r_i}^r \frac{\left(y^4 - r_i^4 + 4 \cdot y^4 \cdot \ln\left(\frac{r_i+w}{y}\right) \right) \cdot (\sin(4 \cdot \phi) + \sin(2 \cdot \theta - 2 \cdot \phi) - \sin(2 \cdot \theta + 2 \cdot \phi))}{32 \cdot y^2} dy - \frac{1}{r} \int_{r_i}^r \frac{\left[4 \cdot \cos(\phi) \cdot \sin(\phi) \cdot (\cos(\theta)^2 - 1) + 4 \cdot \cos(\theta)^2 \cdot \cos(\phi) \cdot \sin(\phi) \right] \cdot \left(r_i^4 - y^4 + 4 \cdot y^4 \cdot \ln\left(\frac{r_i+w}{y}\right) \right)}{16 \cdot y^2} dy$$

Stress sensitivity of SC cables



Courtesy: Emanuela Barzi

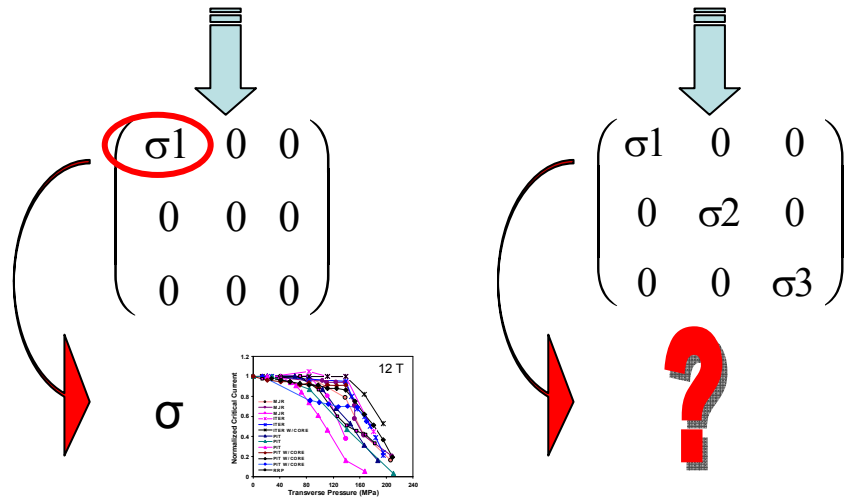
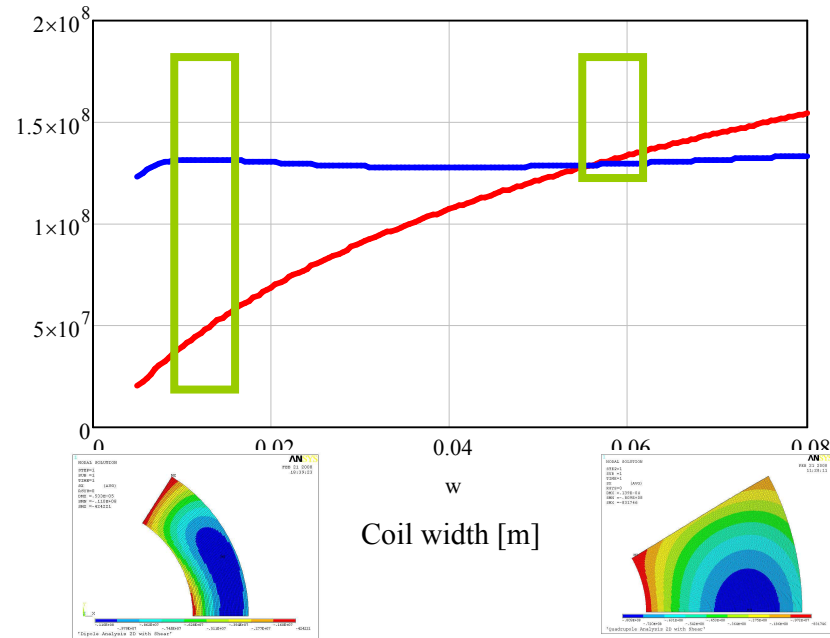
Multiaxiality

Coil Max Stress [Pa]

— $\sigma(r, \theta, z) = \sigma(\text{root}(d, \text{orn}(p, w, r_i, \phi)), p, 0, w, r_i, \phi)$

— $\sigma\theta\left(\text{root}\left(4 \cdot x \cdot \ln\left(\frac{r_i+w}{x}\right) + \frac{r_i^4}{x^3} - x, x\right), 0, w, r_i, \phi\right)$

—



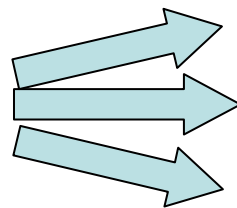
Candidates ϵ_{eq}

- Loss of SC properties is due to crystal lattice deformations
- Strain more meaningful than stress
- Deformations along Cross-Section are critical

2° Order Tensor  Scalar

Candidates:

$$\begin{pmatrix} \epsilon_1 & 0 & 0 \\ 0 & \epsilon_2 & 0 \\ 0 & 0 & \epsilon_3 \end{pmatrix}$$



- Maximum Eigenvalue $\max(\epsilon_i)$
- Maximum Shear: $\max(\epsilon_i - \epsilon_j)$
- Maximum Shear on Cross Section: $\max(\epsilon_1 - \epsilon_2)$

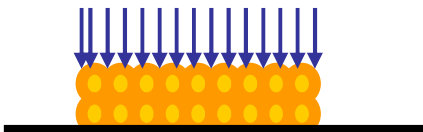
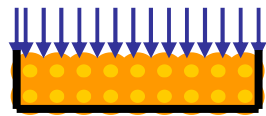
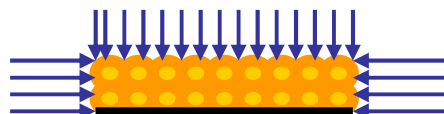
?

Candidates ϵ_{eq}

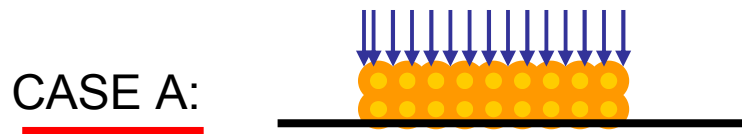


Idea

- A test of the *same cable*
- in **three different multiaxial conditions**,
- and
- *Comparison of the results with those previewed by each model*

CASE A:		$\begin{pmatrix} \nu \frac{p}{E} & 0 & 0 \\ 0 & -\frac{p}{E} & 0 \\ 0 & 0 & \nu \frac{p}{E} \end{pmatrix}$		Now we calculate for each one the three possible equivalent stresses
CASE B:		$\begin{pmatrix} \epsilon_{xx0} & 0 & 0 \\ 0 & (\nu^2 - 1) \frac{p}{E} - \nu \epsilon_{xx0} & 0 \\ 0 & 0 & \nu(1 + \nu) \frac{p}{E} - \nu \epsilon_{xx0} \end{pmatrix}$		
CASE C:		$\begin{pmatrix} \epsilon_{xx0} & 0 & 0 \\ 0 & (\nu^2 - 1) \frac{p}{E} - \nu \epsilon_{xx0} & 0 \\ 0 & 0 & \nu(1 + \nu) \frac{p}{E} - \nu \epsilon_{xx0} \end{pmatrix}$		

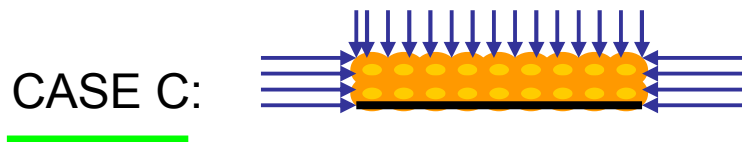
Data interpretation



Hyp 1: Maximum Eigenvalue $\max(\epsilon_i)$

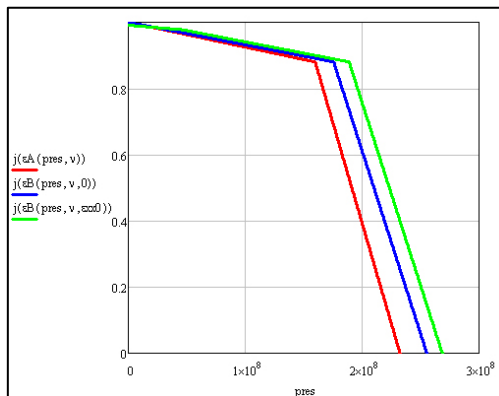


Hyp 2: Maximum Shear: $\max(\epsilon_i - \epsilon_j)$

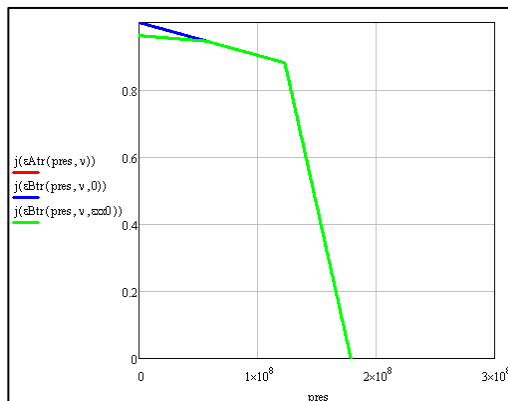


Hyp 3: Maximum Shear on Cross Section: $\text{mod}(\epsilon_1 - \epsilon_2)$

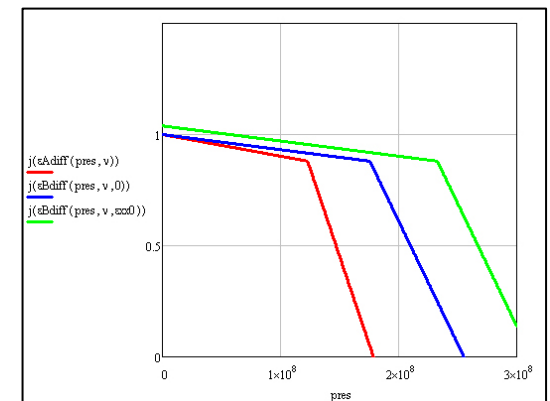
If Hyp1 were true:



If Hyp2 were true:



If Hyp3 were true:



Outline

I. A Parametric Model for Electromechanical Effects in HFMs

- Linear
- Analytic solutions
- Limits of HFMs

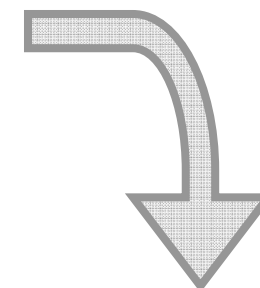


Results suggest the need of

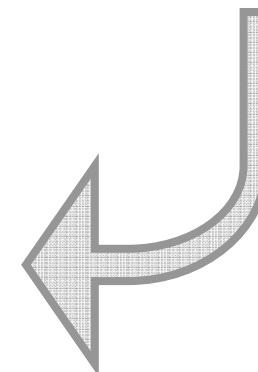
II. An experiment for equivalent stress in HFMs

III. A FEM Elastoplastic Model

- Accuracy of parametric model
- Non-linear phenomena



The P.M. was checked and integrated with

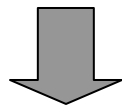


III. A FEM Elastoplastic Model - Outline

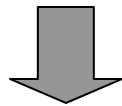
- Introduction
 - Coil preload
 - Training
 - Ratcheting
 - Goals of analysis
- Model description
- Results

Coil Preload

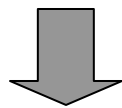
Lorentz Force



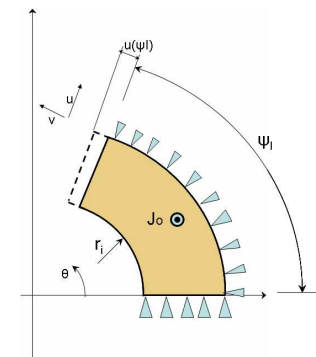
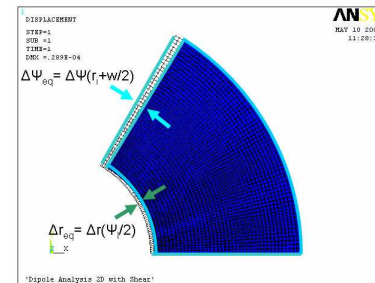
Coil Deformation



Loss of Field Quality

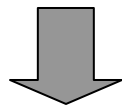


Preload

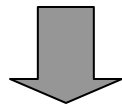


Training

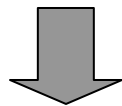
Lorentz Force



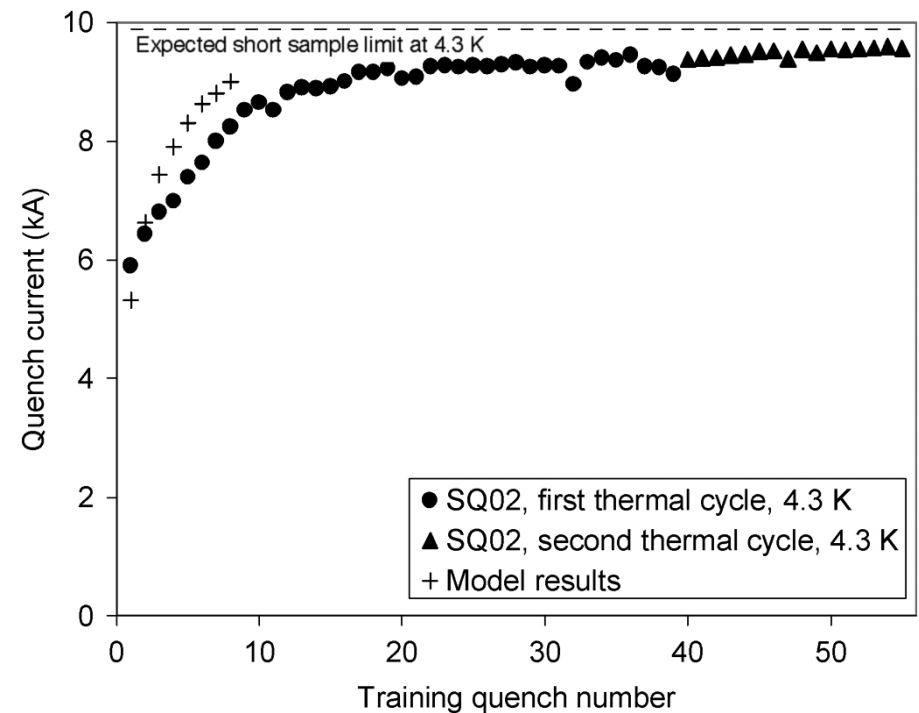
Mechanical Motion



Coil Locked in a more stable position and Hardened



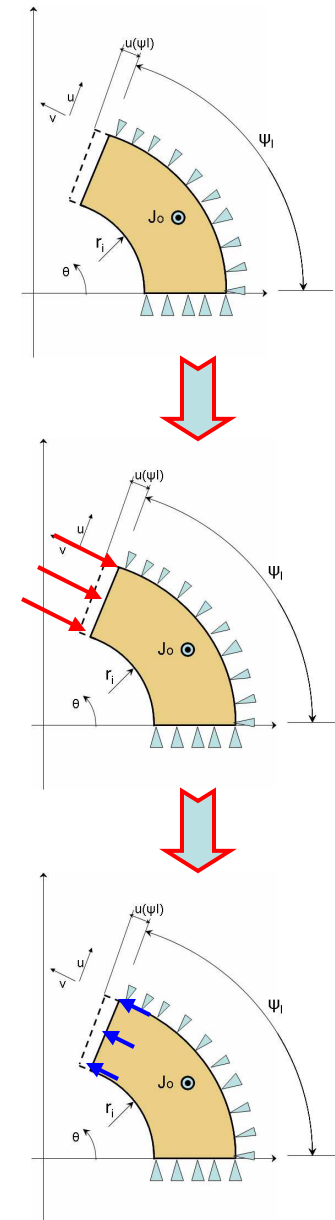
Improvement of quench current



“Spring Back”

The *spring back* occurs when, during the mounting process, the coil is preloaded more than the final configuration.

A device is being developed at LBNL to avoid the *spring back* from occurring.

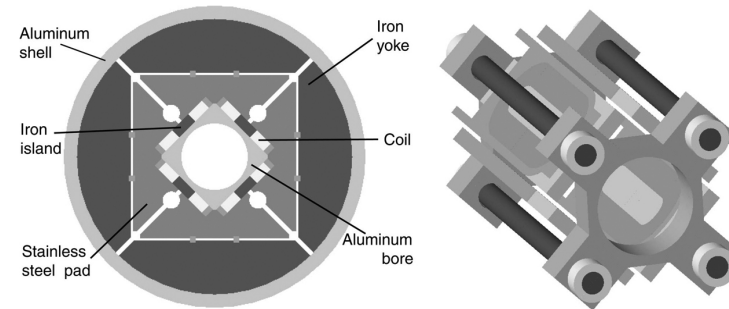


Ratcheting

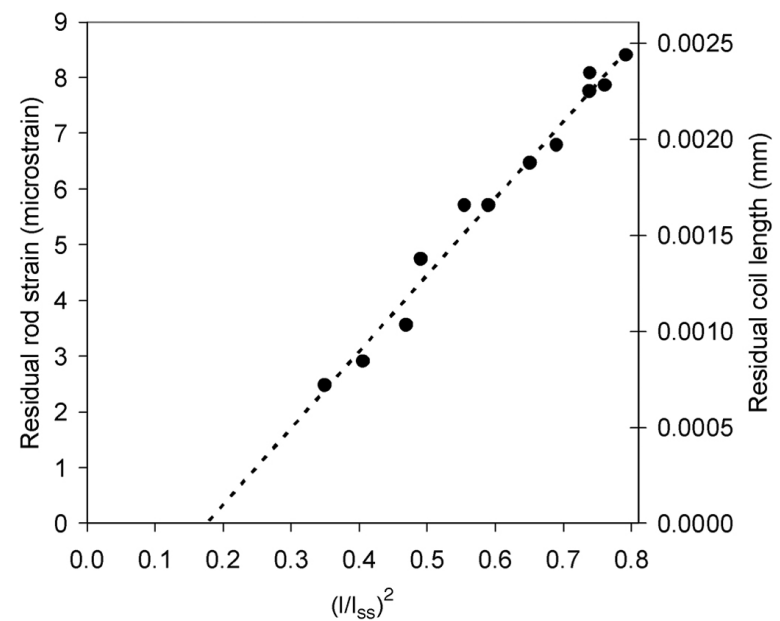
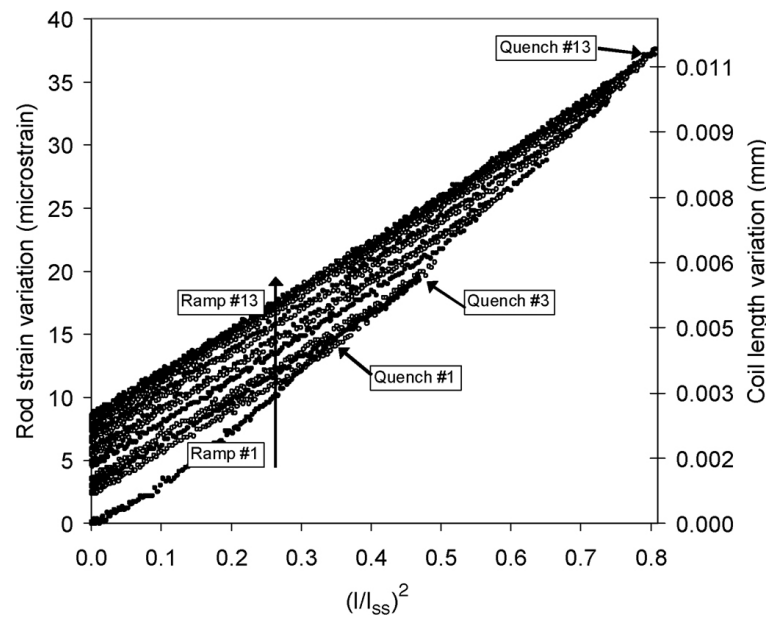
Ratcheting:

After consecutive training ramps, the rods supporting axially the coils show increasing residual strain

(Ferracin 2007)



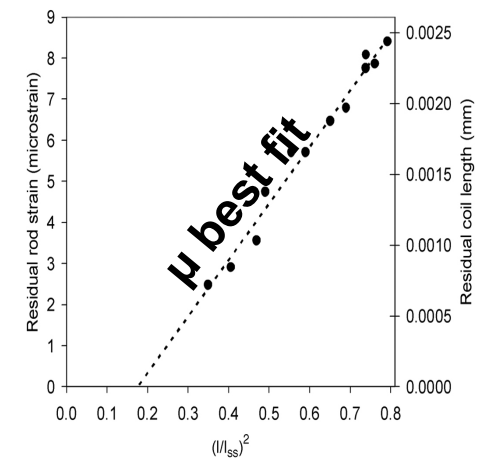
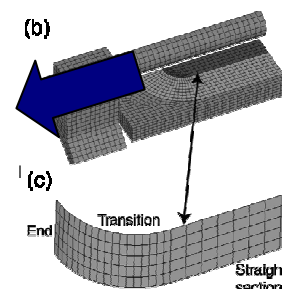
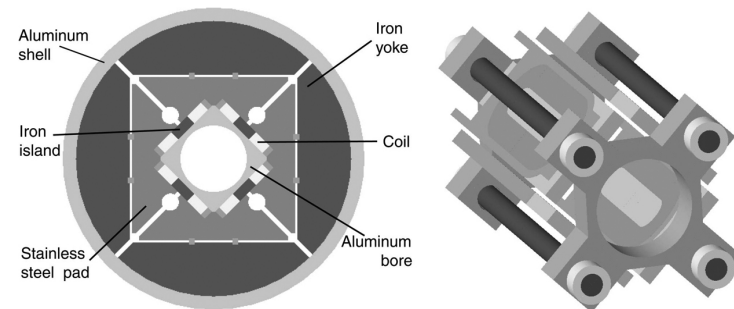
SQ02



Ratcheting

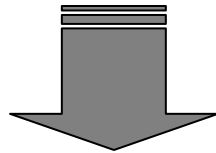
Ferracin, Caspi, Lietzke 2007

- 3D linear FEM model including friction of small racetrack magnet SQ02
- **Axial Lorentz forces** on turns stretch the coil which is then **locked by frictional forces** on the new configuration
- Friction between coil and structure responsible for the residual strain



Goals of analysis

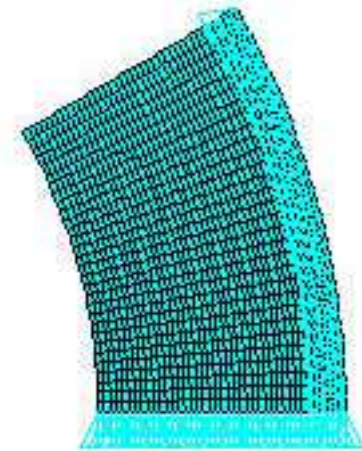
- Role of plastic conservation of volume in coil axial elongation
- Limits of the linear FEM model
- Explanation of the progressive loss of prestress after consecutive training quenches (I. Novitzki et al.)



Elastoplastic FEM Model

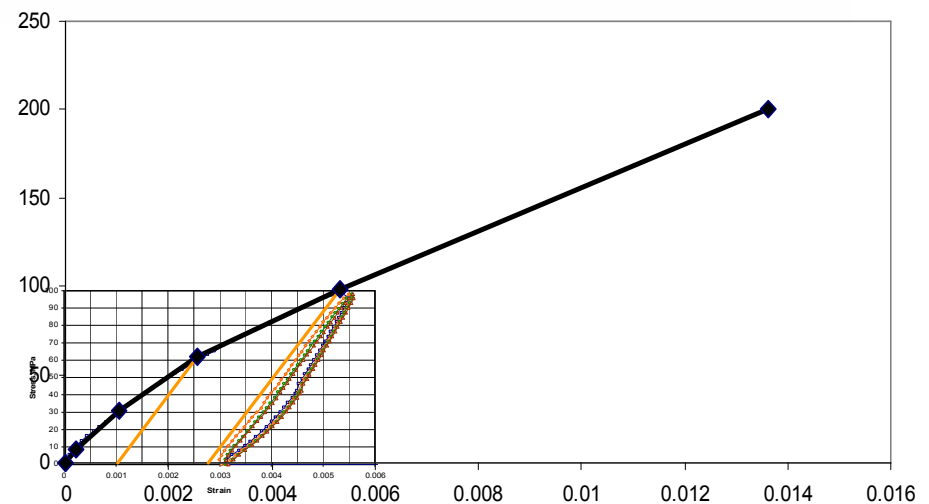
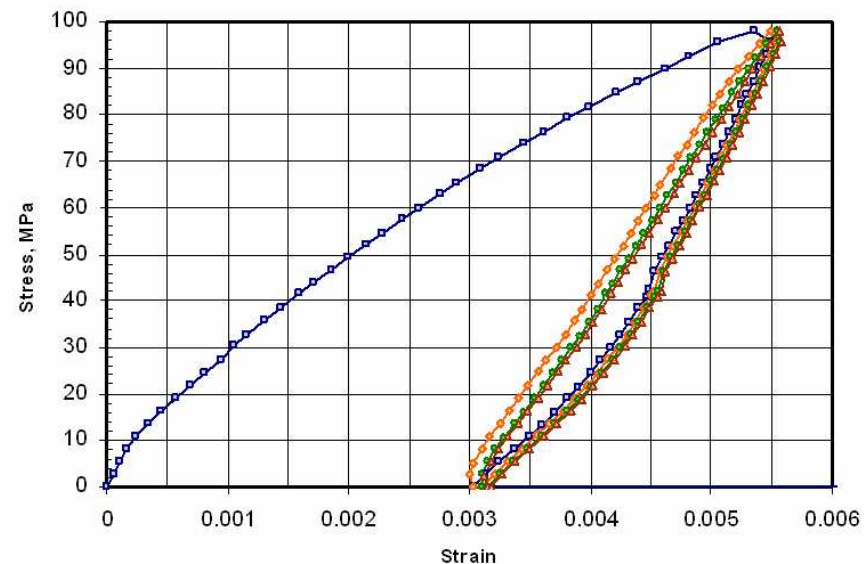
Model - Geometry

- Quadrupole sector,
2D ANSYS element
- 90 mm bore, 20 mm
thickness
- Plane strain,
elastoplastic
behaviour



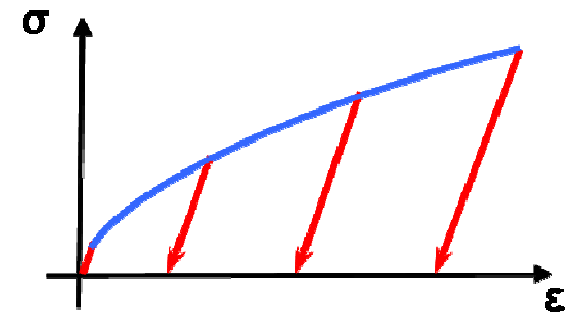
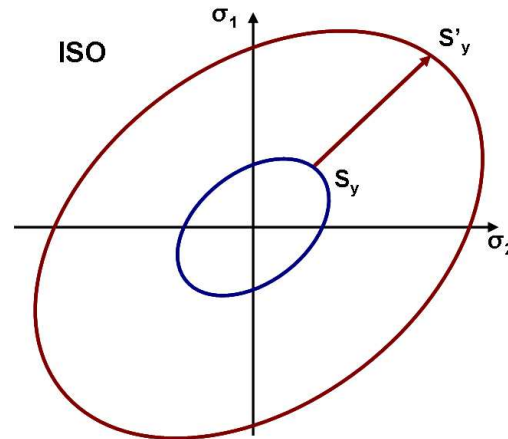
Model – Material Properties

- 6 points multilinear approximation of σ - ε curve
- Data from HFM Dipole, *Fermilab-Conf-99/052* - (D. Chichili)
- Tangent is continued to 200 MPa to extend range

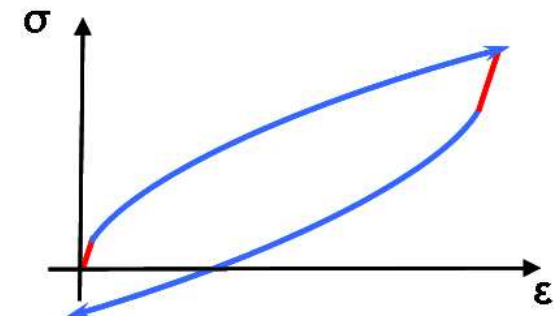
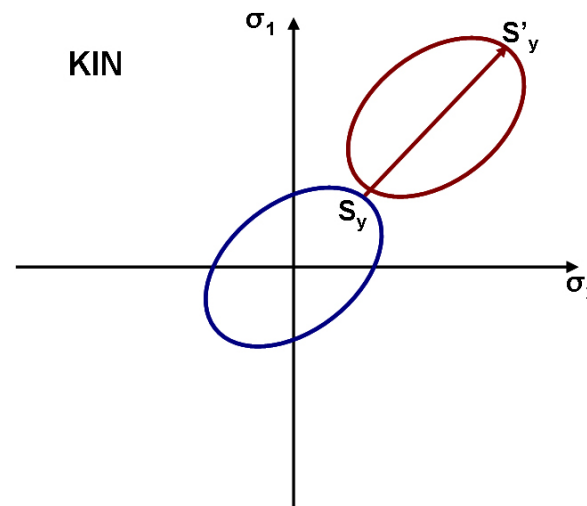


Model – Isotropic hardening Law

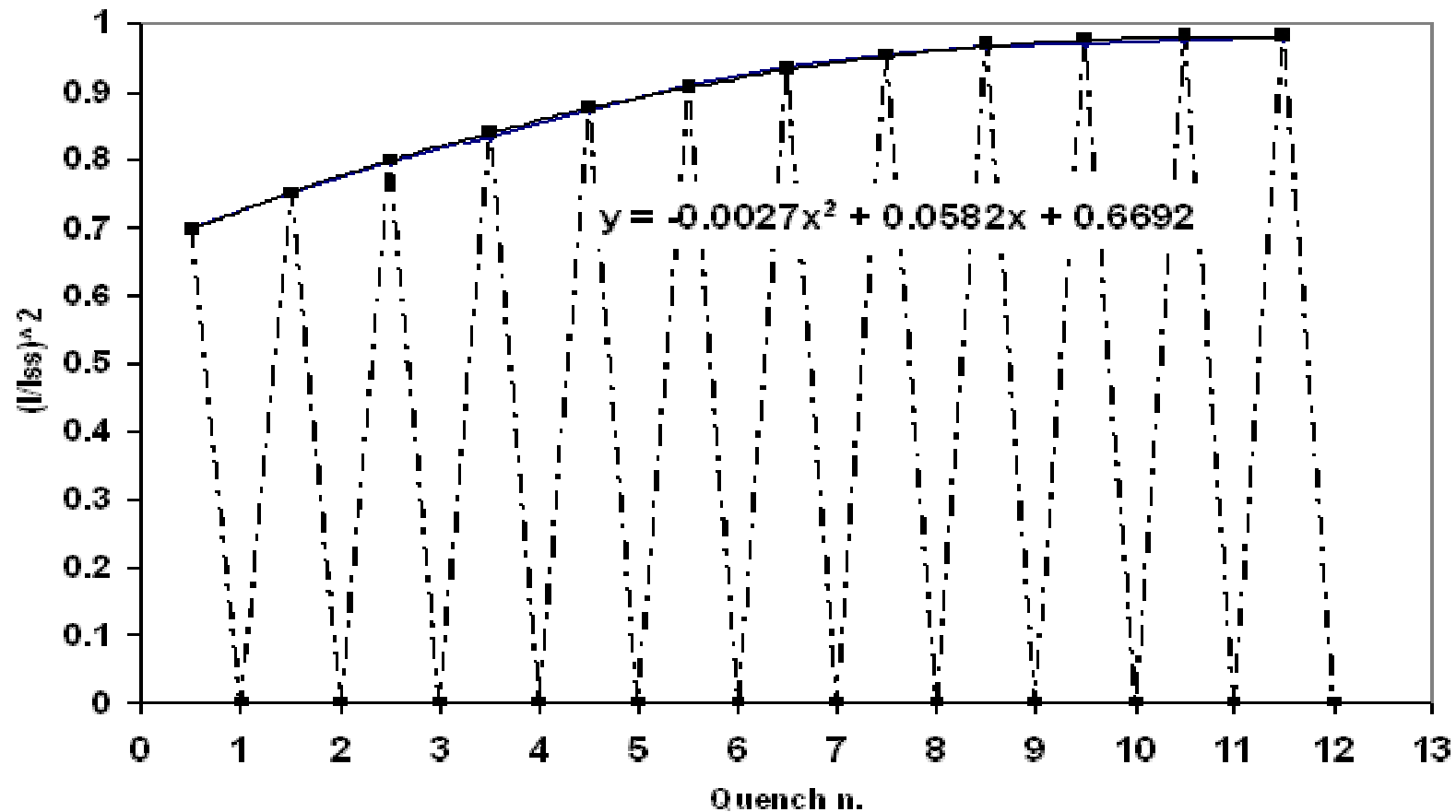
Ansysis: MISO



Ansysis: MKIN
(Metals)



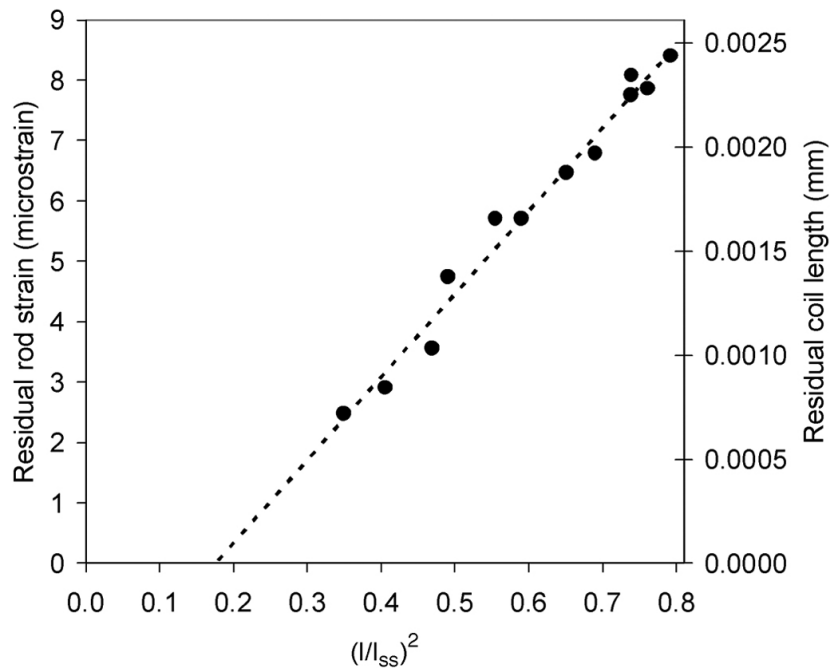
Model - Training



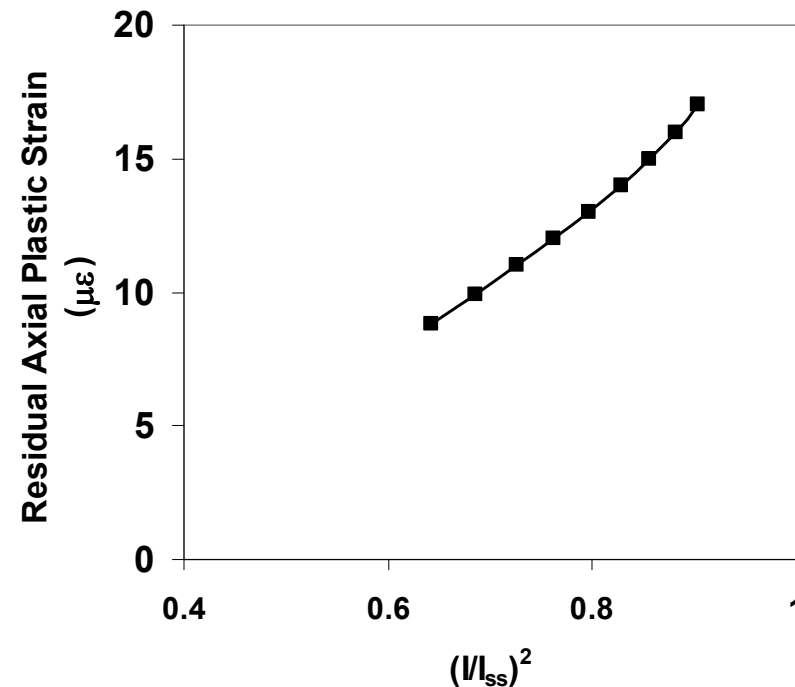
A simplified training curve was approximated with a polynomial. 12 quenches, from 70% to 98% of $ss/$ of parametric model

Results – 1) Residual Axial Strain

SQ02

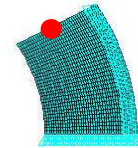
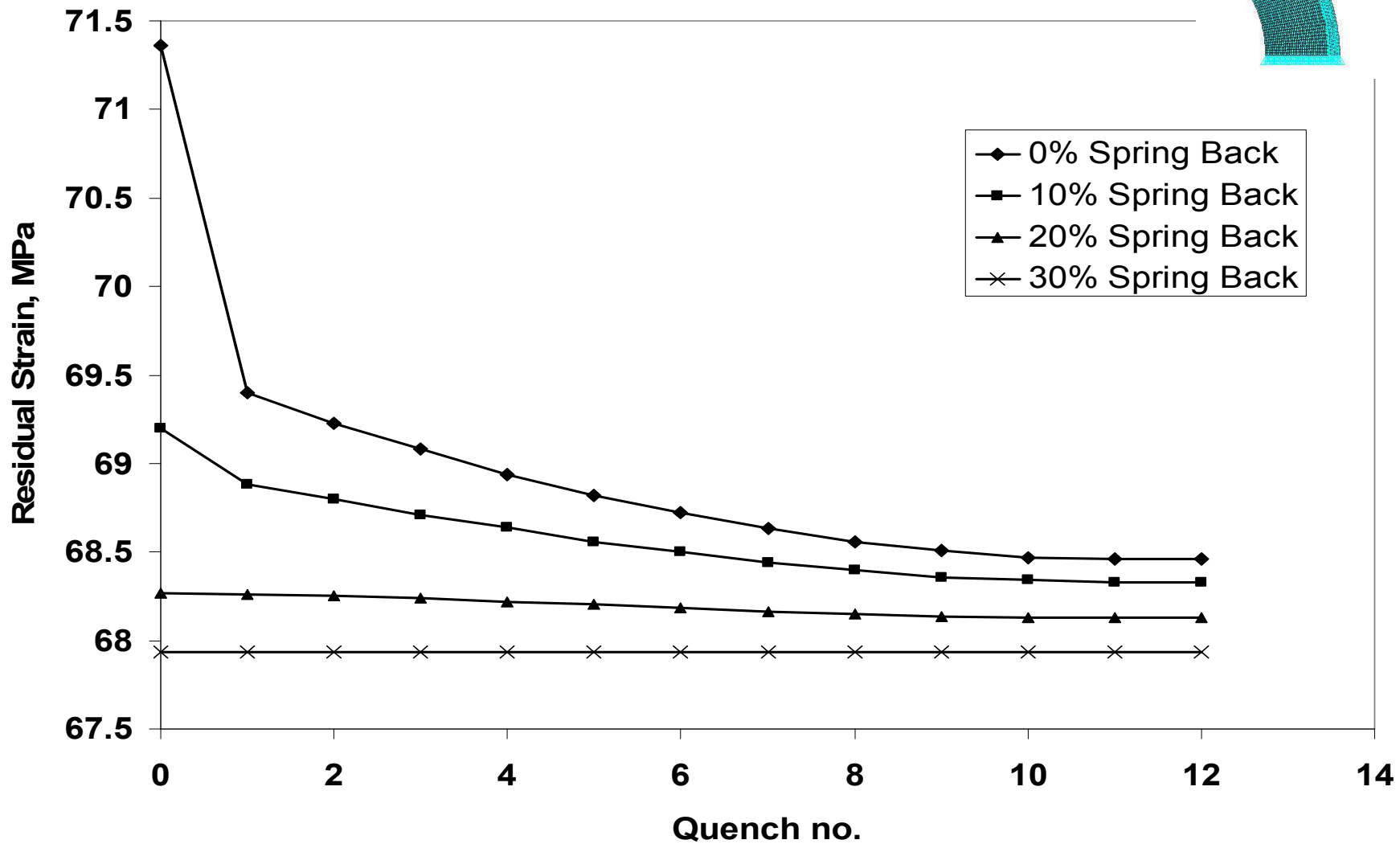


FEM Model

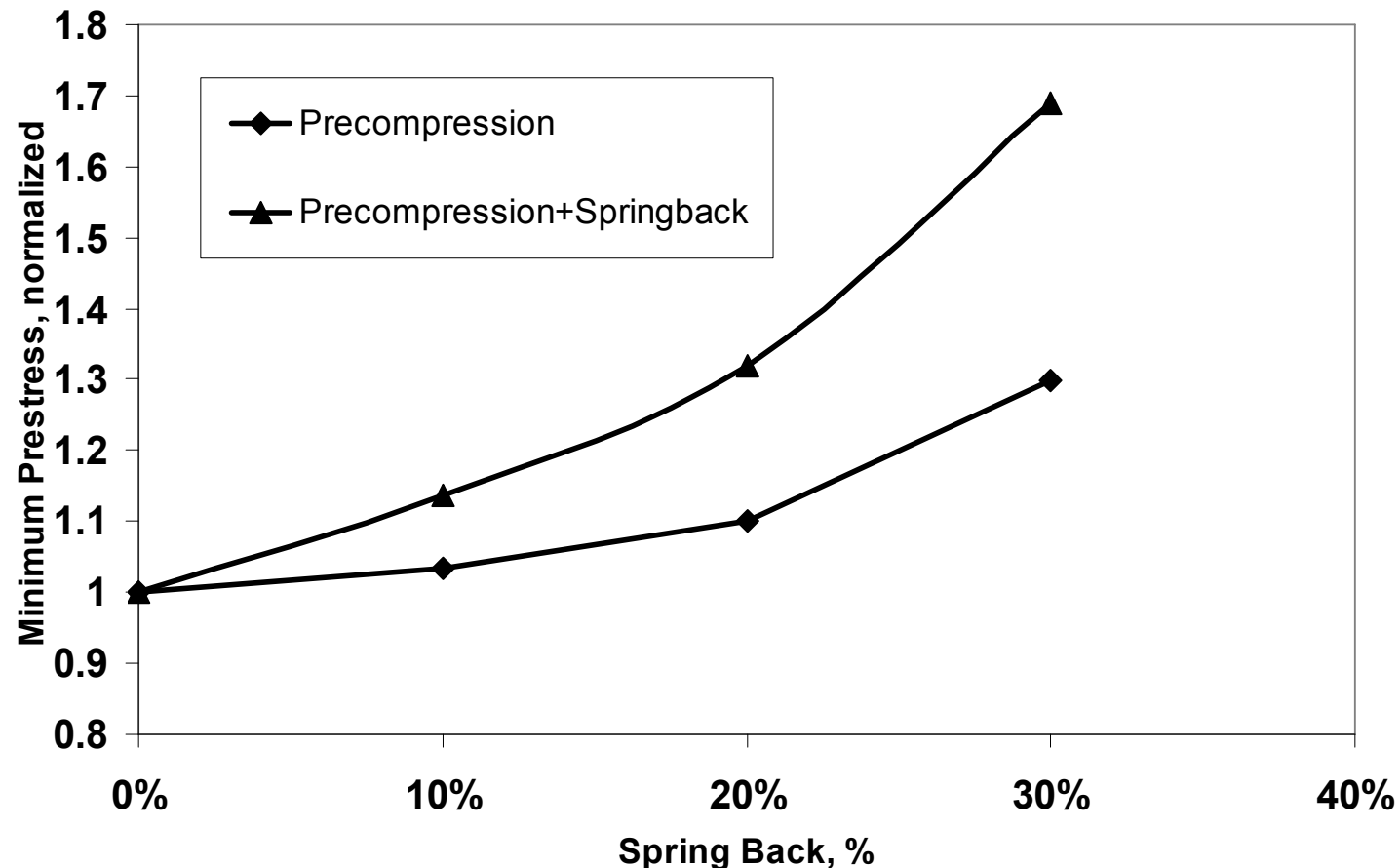


Results suggest that plastic deformations due to cross-sectional loads play an important role in ratcheting.

Results - 2) Loss of Preload



Results - 3) Effect of Springback on Minimum Precompression



The downside of a high springback is the higher minimum precompression required, adding up to the springback

Results - 4) Limits of linear model

- Results prove that stress distribution does not show significant difference between linear and elastoplastic model (<2%)
- Evaluation of minimum precompression should be done with nonlinear model